

Investigating the Mechanistic of Danhong Injection in Brain Damage Caused by Cardiac I/R Injury via Bioinformatics, Computer Simulation, and Experimental Validation

Jinfu Wang,[†] Yan Guo,[†] Huifen Zhou, Yanjie Hua, Haitong Wan,^{*} and Jiehong Yang^{*}



Cite This: *ACS Omega* 2024, 9, 18341–18357



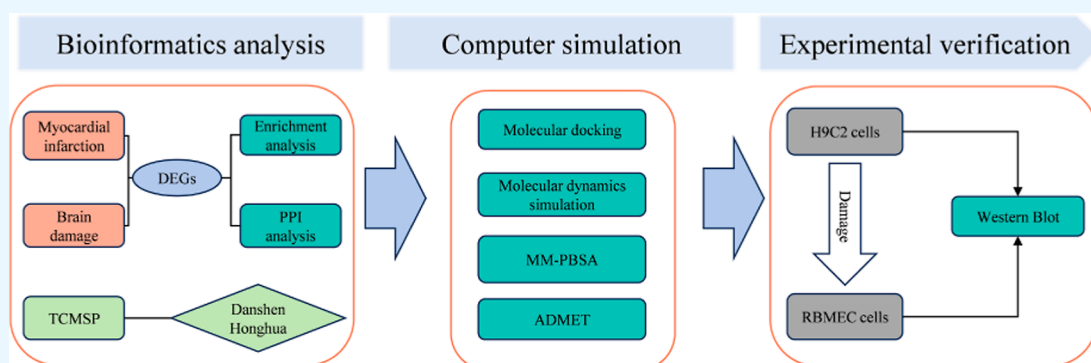
Read Online

ACCESS |

Metrics & More

Article Recommendations

Supporting Information



ABSTRACT: Objective: Cardiac ischemia-reperfusion (I/R) injury has negative effects on the brain and can even lead to the occurrence of ischemic stroke. Clinical evidence shows that Danhong injection (DHI) protects the heart and brain following ischemic events. This study investigated the mechanisms and key active compounds underlying the therapeutic effect of DHI against brain damage induced by cardiac I/R injury. Methods: The gene expression omnibus database provided GSE66360 and GSE22255 data sets. The R programming language was used to identify the common differentially expressed genes (cDEGs). Gene ontology and Kyoto Encyclopedia of Genes and Genomes enrichment analysis were performed, and protein–protein interaction network was constructed. Active compounds of DHI were collected from the Traditional Chinese Medicine Systems Pharmacology database. Molecular docking and molecular dynamics simulations were performed. The MMPBSA method was used to calculate the binding-free energy. The pkCSM server and DruLiTo software were used for Absorption, Distribution, metabolism, excretion, and toxicity (ADMET) analysis and drug-likeness analysis. Finally, in vitro experiments were conducted to validate the results. Results: A total of 27 cDEGs had been identified. The PPI and enrichment results indicated that TNF- α was considered to be the core target. A total of 80 active compounds were retrieved. The molecular docking results indicated that tanshinone I (TSI), tanshinone IIA (TSIIA), and hydroxyl safflower yellow A (HSYA) were selected as core active compounds. Molecular dynamics verification revealed that the conformations were relatively stable without significant fluctuations. MMPBSA analysis revealed that the binding energies of TSI, TSIIA, and HSYA with TNF- α were -36.01 , -21.71 , and -14.80 kcal/mol, respectively. LEU57 residue of TNF- α has the highest contribution. TSI and TSIIA passed both the ADMET analysis and drug-likeness screening, whereas HSYA did not. Experimental verification confirmed that DHI and TSIIA reduced the expression of TNF- α , NLRP3, and IL-1 β in the injured H9C2 and rat brain microvascular endothelial cells. Conclusion: TNF- α can be considered to be a key target for BD-CI/R. TSIIA in DHI exerts a significant inhibitory effect on the inflammatory damage of BD-CI/R, providing new insights for future drug development.

1. INTRODUCTION

With the increase in the aging population and lifestyle changes, there is a rise in the incidence of acute myocardial infarction (AMI) year by year.^{1,2} Reperfusion therapy is the preferred approach for treating AMI. Regrettably, patients often encounter numerous adverse sequelae despite the success of reperfusion.³ Patients with AMI not only face cardiac complications but also encounter varying degrees of brain damage. After the occurrence of cardiac ischemia/reperfusion (I/R) injury, dendritic spine loss leads to the appearance of

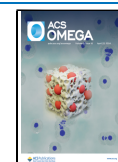
anxiety, depression, insomnia, and even cognitive impairment.^{4–6} The calcium imbalance, inflammatory response, and oxidative stress that occur after cardiac I/R injury gradually

Received: January 7, 2024

Revised: March 22, 2024

Accepted: March 26, 2024

Published: April 11, 2024



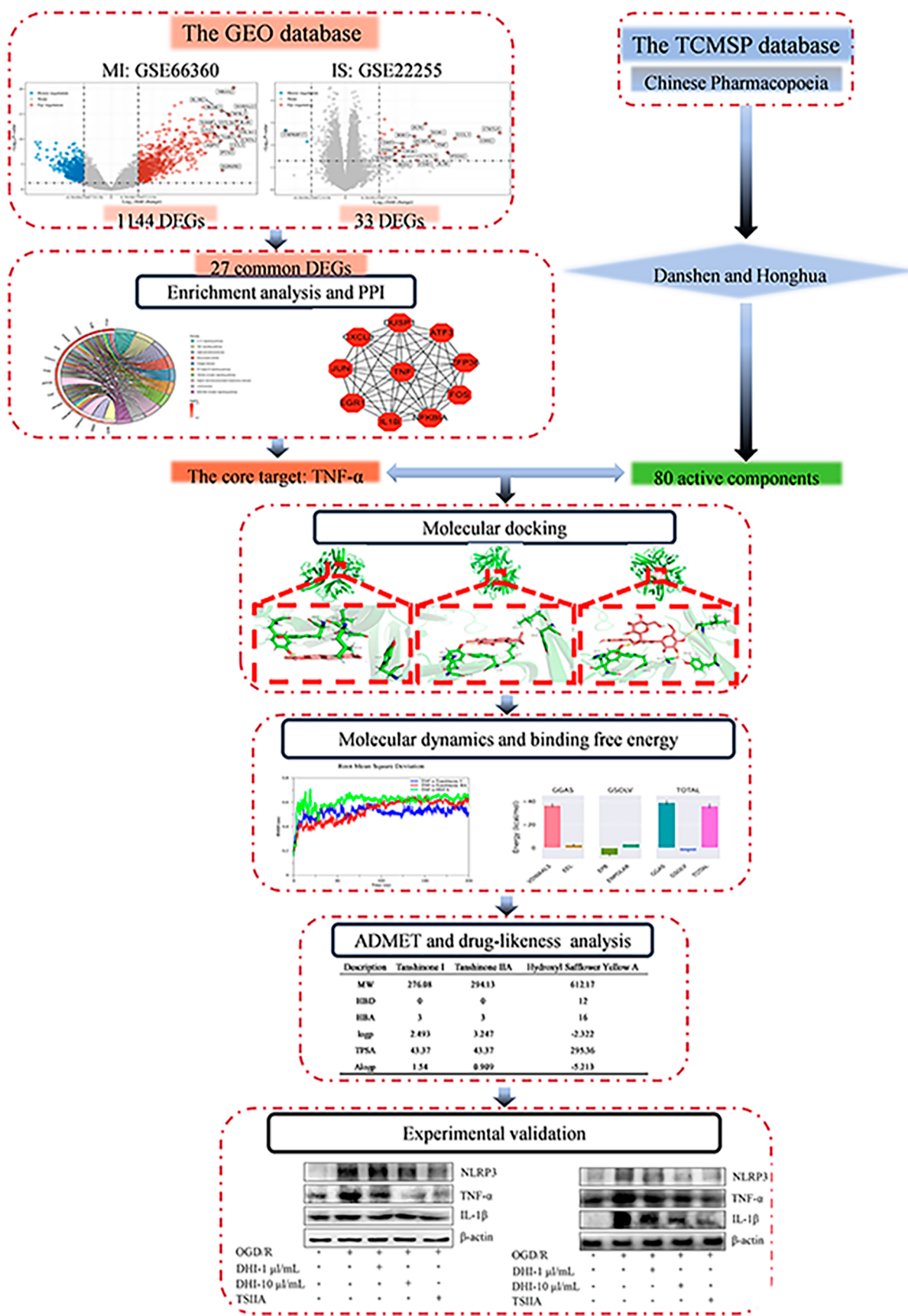


Figure 1. Research flowchart. Read in order from top to bottom.

disrupt the blood–brain barrier (BBB), exacerbating damage to the brain.^{5,7} Ischemic stroke (IS) is one of the most serious

complications. Currently, anti-I/R injury often uses angiotensin-converting enzyme inhibitors, beta-blockers, calcium

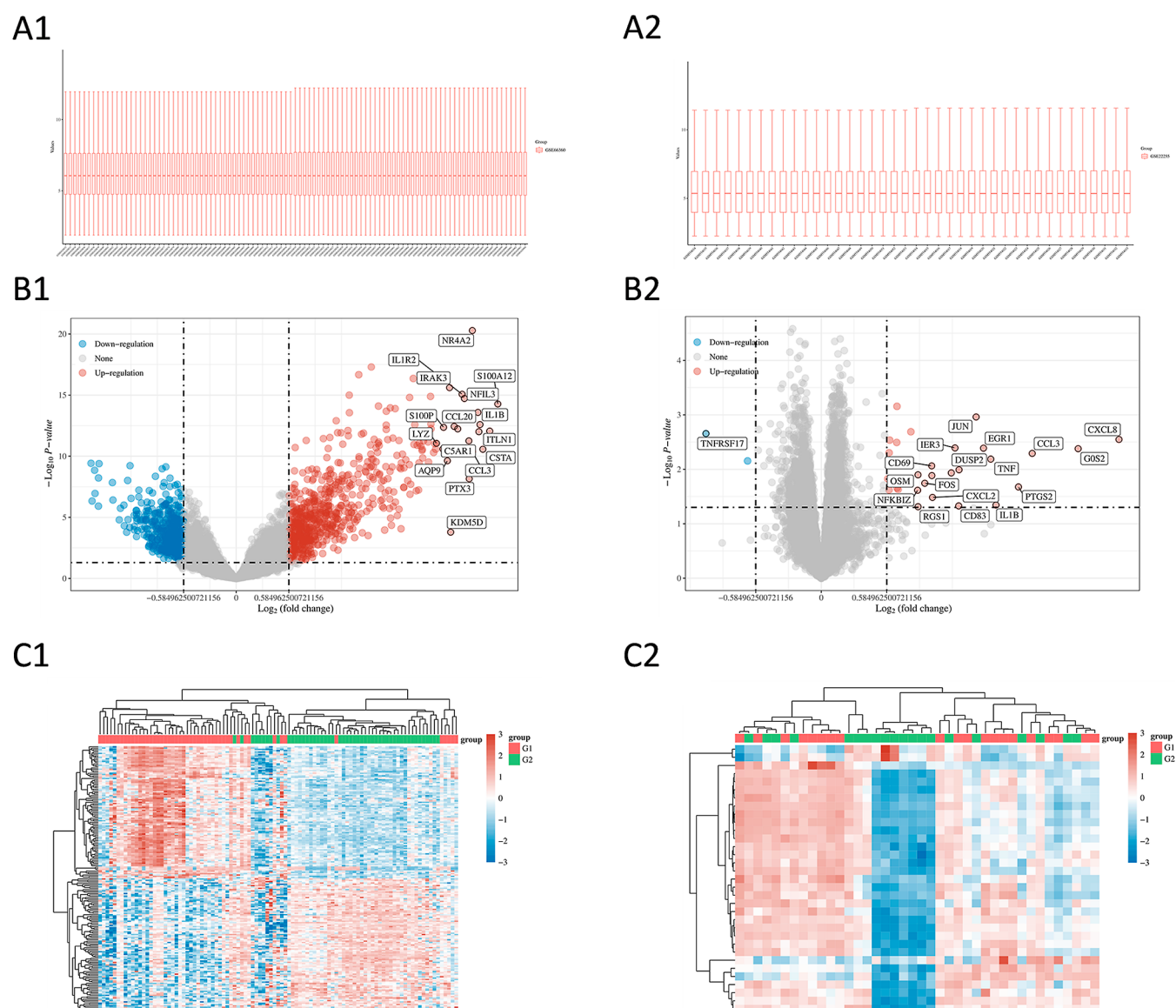


Figure 2. Screening of DEGs. (A1) Data normalization of GSE66360 (MI) analysis. (A2) Data normalization of GSE22255 (IS) analysis. (B1) The volcano plot of MI and (B2) the volcano plot of IS. Upregulated genes are represented in red, downregulated genes are in blue, and no significant difference is indicated by gray. (C1) Heatmap of MI and (C2) heatmap of IS. Heatmaps display the gene expression trends, with rows representing genes and columns representing samples. G1 represents the disease group, while G2 represents the normal group.

channel blockers, and diuretics.^{8,9} These treatment measures can reduce myocardial oxygen consumption, improve heart function to prolong lifespan, but they have side effects such as edema, hyperkalemia, fatigue, and dizziness, which affect the quality of life of patients.⁸ Due to the complexity of the pathogenesis of cardiovascular and cerebrovascular diseases, the existing single treatment methods often fail to meet clinical needs. Therefore, seeking comprehensive treatment methods for brain damage caused by cardiac I/R injury (BD-CI/R) has become a new research focus.

Studies have confirmed that natural ingredients such as flavonoids like quercetin, terpenes like catalpol, polyphenols like resveratrol, saponins like dioscin, derived from herbs, can improve I/R injury through antioxidative, anti-inflammatory, antiapoptotic, and regulation of energy metabolism pathways.^{8,10–12} This indicates that natural products have the comprehensive therapeutic advantage of multiple components, targets, and mechanisms of action. Danhong Injection (DHI)

is composed of *Salviae Miltiorrhizae Radix et Rhizoma*, known as Danshen in Chinese (DS), and *Carthami Flos*, known as Honghua in Chinese (HH). DHI exhibits effects such as antiplatelet coagulation, anti-inflammation, antioxidation, and antiapoptosis.^{13,14} DHI is commonly used for the prevention and treatment of cardiovascular and cerebrovascular diseases.^{15,16} However, further research is needed to investigate the effective active compounds and key mechanisms of action of DHI on BD-CI/R.

Systems pharmacology is an interdisciplinary and integrated research approach with bioinformatics, computational biology, network pharmacology, molecular docking, molecular dynamics, and other techniques.¹⁷ It combines the actions of drugs with biological information at various levels of the biological system to construct and analyze integrative models of the actions of drugs.¹⁸ Additionally, high-throughput sequencing technologies and microarray chip technologies have facilitated the establishment of gene expression profiles of diseases.¹⁹ In

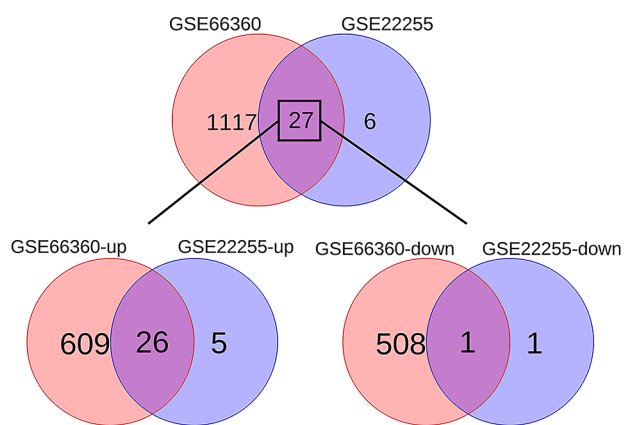


Figure 3. Screening of common differentially expressed genes (cDEGs) of brain damage caused by cardiac I/R injury. The Venn diagram shows a total of 27 cDEGs, consisting of 26 upregulated genes and 1 downregulated gene.

Table 1. cDEGs of BD-CI/R

cDEGs	log ₂ FC of MI	log ₂ FC of IS	average log ₂ FC	regulation
JUN	1.668	1.382	1.525	up
ZFP36	1.928	0.800	1.364	up
CXCL8	1.377	2.658	2.018	up
DUSP1	0.953	0.611	0.782	up
NFKBIA	1.742	0.673	1.208	up
IER3	2.035	1.194	1.615	up
EGR1	1.046	1.448	1.247	up
GOS2	1.248	2.293	1.771	up
CCL3	2.625	1.883	2.254	up
TNF	1.193	1.513	1.353	up
DUSP2	0.890	1.230	1.060	up
PPP1R15A	1.986	1.161	1.573	up
OSM	0.871	0.864	0.868	up
TNFAIP3	1.282	0.988	1.135	up
CDKN1A	1.590	0.629	1.109	up
FOS	2.032	0.924	1.478	up
PTGS2	1.402	1.761	1.581	up
JUNB	0.842	0.677	0.760	up
DDIT4	0.809	0.686	0.748	up
ATF3	0.778	0.605	0.691	up
NFKBIZ	1.362	0.860	1.111	up
CXCL2	1.977	0.993	1.485	up
SOD2	1.572	0.598	1.085	up
IL1B	2.688	1.560	2.124	up
CD83	2.217	1.227	1.722	up
RGS1	1.232	0.864	1.048	up
TNFRSF17	-0.930	-1.030	-0.980	down

this study, we aimed to determine the key active compounds of DHI and identify the key targets for treating BD-CI/R through bioinformatics, computer simulation, and experimental validation (The workflow of this study is shown in Figure 1).

2. MATERIALS AND METHODS

2.1. Tools, Databases, and Reagents. Gene Expression Omnibus (GEO): <http://www.ncbi.nlm.nih.gov/geo/>; BioLadder platform: <https://www.bioladder.cn/>; Metascape: <https://metascape.org/>; STRING: <https://string-db.org/>; UniProt: <https://www.uniprot.org/>; TCMSP: [https://old.tcmsp-e.com/tcmsp.php](https://old.tcm-sp-e.com/tcmsp.php); RCSB Protein Data Bank (RCSB PDB): <https://www.rcsb.org/>; PubChem: <https://pubchem.ncbi.nlm.nih.gov/>; CgenFF: <https://cgenff.silcsbio.com/>; pkCSM: <https://biosig.lab.uq.edu.au/pkcsm/>; Drug Likeness Tool (DruLiTo): https://nipr.gov.in/pi_dev_tools/DruLiToWeb/DruLiTo_index.html; limma package v3.40.2 of R software; AutoDock Tools v1.5.7; AutoDock Vina v1.2.3; Cytoscape v3.9.1; PyMOL v2.4.0 Open-Source; Discovery Studio Visualizer v21.1.0.20298; GROMACS software package 2022.2; Avogadro v1.2.0; QtGrace v0.2.7; DHI (China Food and Drug Administration Permission Number: Z20026866, Shangdong Heze Buchang Pharmaceutical Co., Ltd., China.); TSIA (CAS NO. 568-72-9, Shanghai Aladdin Biochemical Technology Co., Ltd., China.); Anti-TNF- α antibody (Cat no. 17590-1-AP, Proteintech Group, Inc., Wuhan, China.); Anti-IL-1 β antibody (Cat no. 16806-1-AP, Proteintech Group, Inc., Wuhan, China.); Anti-NLRP3 antibody (Cat no. ab270449, Abcam Biocompany Cambridge, MA, USA).

2.2. Identifying of Potential Gene Targets of Brain Damage Caused by Cardiac I/R Injury. Related data sets were obtained from the GEO database. The GEO database is an international public storage, which collects gene expression data from various organisms, including high-throughput microarray and next-generation sequencing data.²⁰ The data sets were analyzed for differentially expressed genes (DEGs) using the Limma software package in R software. DEGs were determined to correct the false positive results by applying $P < 0.05$ and $|\log_2FC| > 0.585$.²¹ Subsequently, volcano and heat maps were generated separately. The DEGs were uploaded to the BioLadder platform to generate a Venn diagram. According to the Venn diagram, the common DEGs (cDEGs) between cardiac I/R injury and brain damage were acquired.

2.3. Gene Ontology and Kyoto Encyclopedia of Genes and Genomes Enrichment Analysis. Gene ontology (GO) and Kyoto Encyclopedia of Genes and Genome (KEGG) enrichment analyses are bioinformatics methods to functionally analyze a gene set by identifying genes associated with specific biological processes (BP) and pathways. Metascape database²² is an efficient tool for gene analysis in the era of big data. The cDEGs of BD-CI/R were uploaded to the Metascape platform, with the organism set as human and $P < 0.05$ as the threshold.²³ The results were visualized and analyzed by using the BioLadder platform.

2.4. Protein–Protein Interaction Network Construction. Protein–protein interaction (PPI) analysis is utilized to systematically analyze and reveal the interaction relationships between proteins. The cDEGs were uploaded to the STRING database²⁴ for PPI analysis, where unconnected targets were eliminated and other parameters were kept at default settings. Visualization analysis and screening of the core target were performed using Cytoscape v3.9.1 software.

2.5. Collection of Active Compounds. TCMSP database,²⁵ a comprehensive pharmacology database of traditional Chinese medicines, currently collects 499 herbs and 12,144 compounds at the time of writing this paper. It was utilized to collect the active compounds of DS and HH separately with screening criteria of $OB \geq 30$ and $DL \geq 0.18$.²⁵ Additional active compounds were supplemented by referring to the testing standards for DS and HH in the Chinese Pharmacopoeia.²⁶

2.6. Molecular Docking Screening. Molecular docking can predict the binding modes and affinity between drug molecules and protein receptors.²⁷ The 3D crystal structure of the protein target was obtained from the PDB database.²⁸ The preprocessed protein target was added hydrogens using

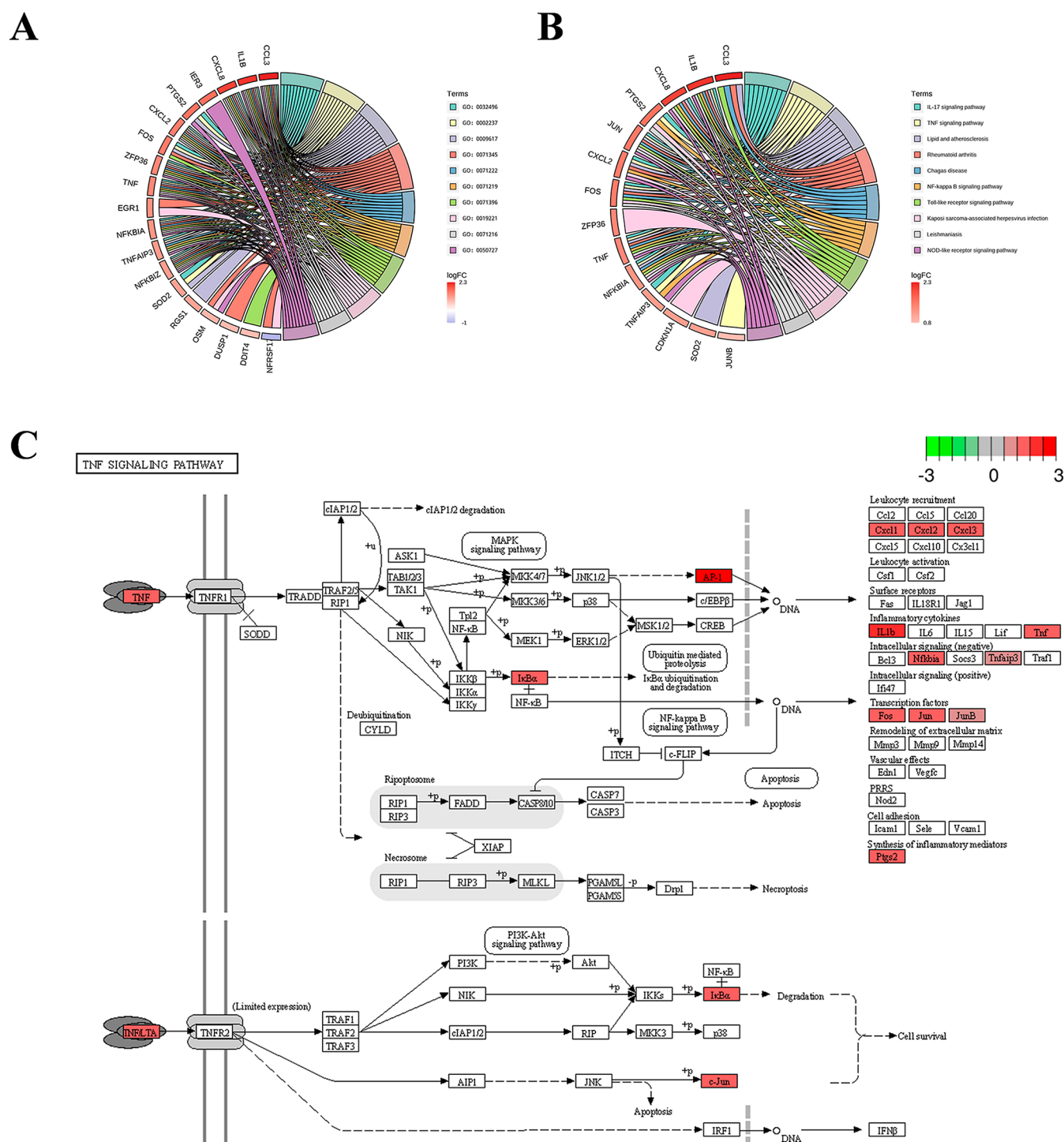


Figure 4. Results of enrichment analysis. (A–B) The chord diagrams of the top 10 entries in the GO and KEGG enrichment analysis. (C) The map of the TNF signaling pathway. Red indicates upregulated genes, while green represents downregulated genes.

AutoDock Tools v1.5.7 and set as the receptor with pdbqt format. A protein grid box was constructed to define a specific volume space within the protein structure and to limit the active site area for docking. To proceed, 3D structure files of active compounds were obtained from the PubChem platform.²⁹ Active compounds, after adding hydrogens, were calculated as atomic charges and then converted into pdbqt format. Finally, molecular docking was performed using AutoDock Vina v1.2.3. The results were visually analyzed using PyMOL v2.4.0 and Discovery Studio v21.1.0 software.

2.7. Molecular Dynamics Simulation. Molecular dynamics is an interdisciplinary technique that is particularly important in studying the interactions between proteins and ligands.³⁰ It is based on Newtonian classical mechanics and is widely used for molecular research.³¹ Molecular dynamics simulations were performed using the GROMACS software package, based on the results obtained from molecular docking.³² The CHARMM36 force field was used for protein topology analysis. The TIP3P water model was chosen to build the topology. Ligand atoms were reordered using Avogadro

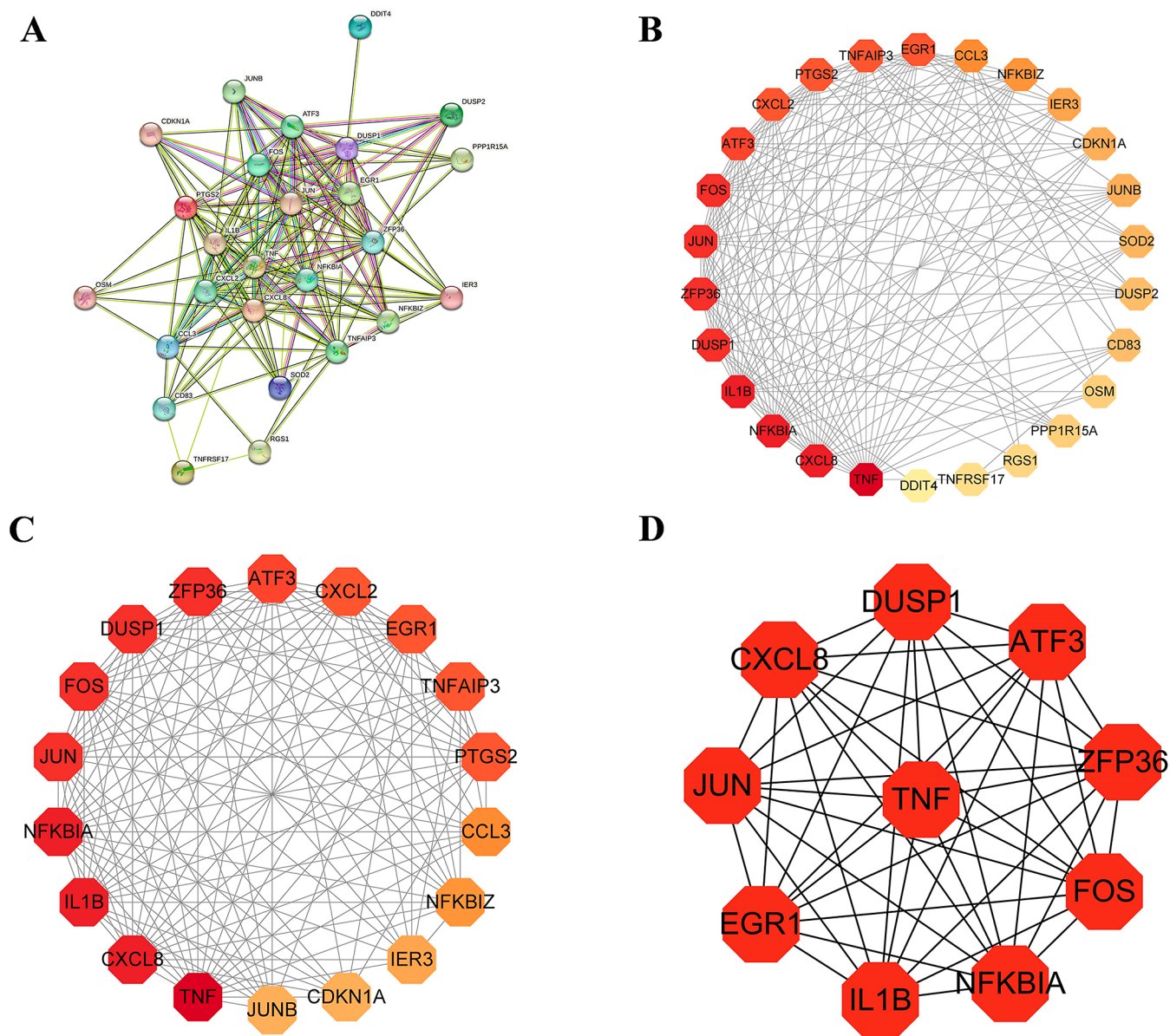


Figure 5. PPI network. (A) PPI network obtained from STRING analysis. (B,C) PPI network from CytoNCA plugin and MCODE plugin, respectively, with darker colors indicating higher node importance. (D) PPI network with the top 10 targets from the cytoHubba plugin analysis.

version 1.2.0 before uploading to the CGenFF server to obtain topology information. The system of the protein–ligand complex was constructed and solvated in a dodecahedral box, with the box boundary set at a distance of 1.2 nm from the solute. Ions such as chloride or sodium were added to neutralize charge deviations. Energy minimization was performed using the steepest descent algorithm with maximum steps of 50,000. The temperature and pressure were maintained at 300 K and 1.0 bar using the Berendsen thermostat and Parrinello–Rahman barostat.³³ Subsequently, 200 ns molecular dynamics simulations were conducted, and the results were visualized by using QtGrace v027 software.

2.8. Calculation of Binding-Free Energy. Obtain the trajectories of the final 1 ns from the molecular dynamics simulation system.^{34,35} The molecular mechanics Poisson–Boltzmann surface area (MM-PBSA) method³⁶ was utilized to evaluate the stability and calculate the binding free energy. The ipb = 2 model was used for the calculation, as it can more accurately describe the charge distribution on the protein

surface and solvation effects. The binding free energy was calculated using the following equation³⁷

$$\Delta G(\text{bind}) = \Delta G(\text{complex}) - [\Delta G(\text{receptor}) + \Delta G(\text{ligand})]$$

Where $\Delta G(\text{complex})$ represents the free energy of the protein–ligand complex, $\Delta G(\text{receptor})$ represents the free energy of the protein, and $\Delta G(\text{ligand})$ represents the free energy of the ligand. Additionally, an energy decomposition analysis was performed to calculate the per-residue energy contributions in the binding site region to ligand binding.

2.9. Exploring the Bioavailability and Toxicity of Active Compounds. Absorption, distribution, metabolism, excretion, and toxicity properties (ADMET) analysis has the potential to minimize research costs and decrease the probability of failure in subsequent animal and clinical experiments. Based on the molecular docking results, the active compounds were uploaded to the pkCSM server³⁸ for

Table 2. 80 Active Ingredients of Danshen-Honghua

Mol ID	molecule name	Mol ID	molecule name
MOL001601	1,2,5,6-tetrahydrotanshinone	MOL007120	miltionone II
MOL001659	poriferasterol	MOL007121	miltipolone
MOL001771	poriferast-5-en-3beta-ol	MOL007122	miltirone
MOL001942	isoimperatorin	MOL007124	neocryptotanshinone ii
MOL002222	sugiol	MOL007125	neocryptotanshinone
MOL002651	dehydrotanshinone II A	MOL007127	1-methyl-8,9-dihydro-7H-naphtho[5,6-g]benzofuran-6,10,11-trione
MOL002776	baicalin	MOL007130	prolithospermic acid
MOL000569	digallate	MOL007132	(2R)-3-(3,4-dihydroxyphenyl)-2-[(Z)-3-(3,4-dihydroxyphenyl)acryloyl]oxy-propionic acid
MOL000006	luteolin	MOL007141	salvianolic acid g
MOL007036	5,6-dihydroxy-7-isopropyl-1,1-dimethyl-2,3-dihydrophenanthren-4-one	MOL007142	salvianolic acid j
MOL007041	2-isopropyl-8-methylphenanthrene-3,4-dione	MOL007143	salvilenone I
MOL007045	3 α -hydroxytanshinoneIIa	MOL007145	salviolone
MOL007048	(E)-3-[2-(3,4-dihydroxyphenyl)-7-hydroxy-benzofuran-4-yl]acrylic acid	MOL007150	(6S)-6-hydroxy-1-methyl-6-methylol-8,9-dihydro-7H-naphtho[8,7-g]benzofuran-10,11-quinone
MOL007049	4-methylenemiltirone	MOL007151	tanshindiol B
MOL007050	2-(4-hydroxy-3-methoxyphenyl)-5-(3-hydroxypropyl)-7-methoxy-3-benzofurancarboxaldehyde	MOL007152	przewaquinone E
MOL007058	Formyltanshinone	MOL007154	tanshinone iia
MOL007059	3-beta-hydroxymethylenetanshinquinone	MOL007155	(6S)-6-(hydroxymethyl)-1,6-dimethyl-8,9-dihydro-7H-naphtho[8,7-g]benzofuran-10,11-dione
MOL007061	methylenetanshinquinone	MOL007156	tanshinone VI
MOL007063	przewalskin a	MOL000098	quercetin
MOL007064	przewalskin b	MOL000358	beta-sitosterol
MOL007068	przewaquinone B	MOL000422	kaempferol
MOL007069	przewaquinone c	MOL000449	stigmaterol
MOL007070	(6S,7R)-6,7-dihydroxy-1,6-dimethyl-8,9-dihydro-7H-naphtho[8,7-g]benzofuran-10,11-dione	MOL000953	CLR
MOL007071	przewaquinone f	MOL002694	4-[(E)-4-(3,5-dimethoxy-4-oxo-1-cyclohexa-2,5-dienylidene)but-2-enylidene]-2,6-dimethoxycyclohexa-2,5-dien-1-one
MOL007077	sclareol	MOL002695	lignan
MOL007079	tanshinaldehyde	MOL002710	pyrethrin II
MOL007081	danshenol B	MOL002712	6-hydroxykaempferol
MOL007082	danshenol A	MOL002714	baicalein
MOL007085	salvilenone	MOL002717	qt_carthamone
MOL007088	cryptotanshinone	MOL002721	quercetagetin
MOL007093	dan-she-xin-kum d	MOL002757	7,8-dimethyl-1H-pyrimido[5,6-g]quinoxaline-2,4-dione
MOL007094	danshenspiroketallactone	MOL002773	beta-carotene
MOL007098	deoxyneocryptotanshinone	MOL007134	danshensu
MOL007100	dihydrotanshinolactone	MOL007157	tanshinone i
MOL007101	dihydrotanshinoneI	MOL007074	salvianolic acid b
MOL007105	epidanshenspiroketallactone	MOL002690	hydroxysafflor-yellow-A
MOL007107	C09092	MOL001452	protocatechualdehyde
MOL007108	isocryptotanshi-none	MOL007136	salvianolic acid a
MOL007111	isotanshinone II	MOL007138	salvianolic acid d
MOL007115	manool		
MOL007119	miltionone I		

computational analysis. The outcomes were then presented in a chart format.

2.10. Drug-Likeness Analysis. Drug-likeness of the core active compounds was analyzed using DruLiTo software and screened according to Lipinski's rule.³⁹ Lipinski's rule generally refers to active compounds with molecular weight (MW) less than 500 Da, hydrogen bond donors (HBD) no more than 5, hydrogen bond acceptors (HBA) no more than 10, logarithmic partition coefficient (log *P*) no greater than 5.⁴⁰ Moreover, topological polar surface area (TPSA) and Atom-based Logarithm of the partition coefficient (Alog *P*) were also analyzed.^{41,42}

2.11. Experimental Verification. 2.11.1. H9C2 Cells and Treatments. The H9C2 cells were cultivated in DMEM medium supplemented with 10% FBS, within a CO₂ cell

incubator set at 37 °C. The cells were randomly divided into five groups: control group, oxygen-glucose deprivation/reperfusion (OGD/R) group, DHI (1 μ L/mL) group, DHI (10 μ L/mL) group, and TSIIA (3 μ M) group. Except for the control group, the cells cultured in MEM medium underwent a 12 h hypoxic treatment in a chamber consisting of 94% N₂, 5% CO₂, and 1% O₂. The supernatant from H9C2 cells after the OGD/R-induced injury was collected for further use. The DHI group and TSIIA group were subsequently treated with DMEM medium containing DHI and TSIIA, respectively, followed by 24 h of incubation under normal oxygen conditions.

2.11.2. Rat Brain Microvascular Endothelial Cells and Treatments. Rat brain microvascular endothelial cells (RBMEC) were grown in a CO₂ cell incubator set at 37 °C

Table 3. Binding-Free Energy Information on Active Compounds with TNF- α

Mol ID	active Ingredient	binding energy (kcal/mol)	Mol ID	active Ingredient	binding energy (kcal/mol)
MOL007093	dan-shexinkum d	-9.882	MOL002757	7,8-dimethyl-1H-pyrimido[5,6-g]quinoxaline-2,4-dione	-8.406
MOL007111	isotanshinone II	-9.676	MOL007136	salvianolic acid a	-8.406
MOL000449	stigmaterol	-9.587	MOL007105	epidanshenspiroketallactone	-8.402
MOL007068	przewaquinone B	-9.493	MOL007045	3 α -hydroxytanshinoneIIa	-8.390
MOL007157	tanshinone i	-9.323	MOL007141	salvianolic acid g	-8.360
MOL001659	poriferasterol	-9.168	MOL007079	tanshinaldehyde	-8.340
MOL007150	(6S)-6-hydroxy-1-methyl-6-methylol-8,9-dihydro-7H-naphtho[8,7-g]benzofuran-10,11-quinone	-9.135	MOL007120	miltionone II	-8.328
MOL007059	3-beta-hydroxymethyltanshinquinone	-9.092	MOL002714	baicalin	-8.317
MOL007101	dihydrotanshinoneI	-9.073	MOL007156	tanshinone VI	-8.205
MOL007061	methylenetanshinquinone	-9.056	MOL007143	salvilene I	-8.130
MOL002773	beta-carotene	-9.046	MOL007122	miltirone	-8.115
MOL002776	baicalin	-9.035	MOL007036	5,6-dihydroxy-7-isopropyl-1,1-dimethyl-2,3-dihydrophenanthren-4-one	-8.023
MOL007069	przewaquinone c	-8.998	MOL002710	pyrethrin II	-8.017
MOL007058	formyltanshinone	-8.988	MOL007107	C09092	-8.011
MOL007152	przewaquinone E	-8.985	MOL007048	(E)-3-[2-(3,4-dihydroxyphenyl)-7-hydroxy-benzofuran-4-yl]acrylic acid	-8.009
MOL007154	tanshinone iia	-8.929	MOL002712	6-hydroxykaempferol	-7.933
MOL007094	danshenspiroketallactone	-8.921	MOL007098	deoxyneocryptotanshinone	-7.932
MOL002651	dehydrotanshinone II A	-8.908	MOL007124	neocryptotanshinone ii	-7.932
MOL001771	poriferast-5-en-3beta-ol	-8.894	MOL007138	salvianolic acid d	-7.927
MOL002721	quercetageitin	-8.881	MOL007142	salvianolic acid j	-7.918
MOL001601	1,2,5,6-tetrahydrotanshinone	-8.875	MOL007119	miltionone I	-7.897
MOL000006	Luteolin	-8.872	MOL007063	przewalskin a	-7.890
MOL007081	danshenol B	-8.869	MOL007125	neocryptotanshinone	-7.819
MOL007082	danshenol A	-8.857	MOL002222	sugiol	-7.800
MOL007070	(6S,7R)-6,7-dihydroxy-1,6-dimethyl-8,9-dihydro-7H-naphtho[8,7-g]benzofuran-10,11-dione	-8.854	MOL002694	4-[(E)-4-(3,5-dimethoxy-4-oxo-1-cyclohexa-2,5-dienylidene)but-2-enylidene]-2,6-dimethoxycyclohexa-2,5-dien-1-one	-7.794
MOL000358	beta-sitosterol	-8.851	MOL001942	isoimperatorin	-7.762
MOL007108	isocryptotanshinone	-8.783	MOL002690	hydroxysafflor-yellow-A	-7.743
MOL007074	salvianolic acid b	-8.771	MOL007130	prolithospermic acid	-7.739
MOL007100	dihydrotanshinlactone	-8.748	MOL000569	Digallate	-7.730
MOL000953	CLR	-8.727	MOL007132	(2R)-3-(3,4-dihydroxyphenyl)-2-[(Z)-3-(3,4-dihydroxyphenyl)acryloyl]oxy-propionic acid	-7.729
MOL007127	1-methyl-8,9-dihydro-7H-naphtho[5,6-g]benzofuran-6,10,11-trione	-8.717	MOL007050	2-(4-hydroxy-3-methoxyphenyl)-5-(3-hydroxypropyl)-7-methoxy-3-benzofurancarboxaldehyde	-7.663
MOL007071	przewaquinone f	-8.708	MOL002717	qt_carthamone	-7.555
MOL007085	salvilene	-8.705	MOL007115	manool	-7.538
MOL007145	salviolone	-8.696	MOL007077	sclareol	-7.523
MOL007151	tanshindiol B	-8.628	MOL000098	quercetin	-7.329
MOL007064	przewalskin b	-8.621	MOL000422	kaempferol	-7.263
MOL007041	2-isopropyl-8-methylphenanthrene-3,4-dione	-8.579	MOL002695	lignan	-7.062
MOL007155	(6S)-6-(hydroxymethyl)-1,6-dimethyl-8,9-dihydro-7H-naphtho[8,7-g]benzofuran-10,11-dione	-8.540			
MOL007088	cryptotanshinone	-8.531			
MOL007121	miltipolone	-8.448			
MOL007049	4-methylenemiltirone	-8.434			

using DMEM medium supplemented with FBS (10%). The cells were allocated into five groups in a random manner: control group, model group, DHI (1 μ L/mL) group, DHI (10 μ L/mL) group, and TSIIA (3 μ M) group. The method of cell-to-cell damage model induced by the transfer of cell supernatant was used to construct an RBMEC injury model caused by myocardial ischemia.⁴³ Apart from the control group, the DMEM culture medium of the remaining groups was replaced with the supernatant from OGD/R-H9C2 cells, and incubated in a 37 °C incubator under normal oxygen conditions for 24 h. Subsequently, the DHI group and TSIIA group were treated with DMEM culture medium containing DHI and TSIIA, while the remaining groups were treated with DMEM culture medium without any drugs. The cells were incubated at 37 °C under normal oxygen conditions for 24 h.

2.11.3. Western Blot. After treatment with drugs, H9C2 cells and RBMEC were collected separately and then washed twice with PBS before being lysed using a RIPA buffer. Total protein was separated by SDS-PAGE and transferred onto a PVDF membrane. After the transfer of proteins, a blocking step was carried out using a 1 \times TBST solution fortified with nonfat milk powder (5%) at room temperature for 2 h. Subsequently, the samples were incubated with the primary antibody overnight at 4 °C. On the subsequent day, the membrane was washed three times with TBST, followed by incubation with the corresponding secondary antibody (mouse or rabbit) at room temperature for 1 h. Finally, the images were captured using a chemiluminescence imaging system (Azure Biosystems, Dublin, USA) and subsequently analyzed with ImageJ software.

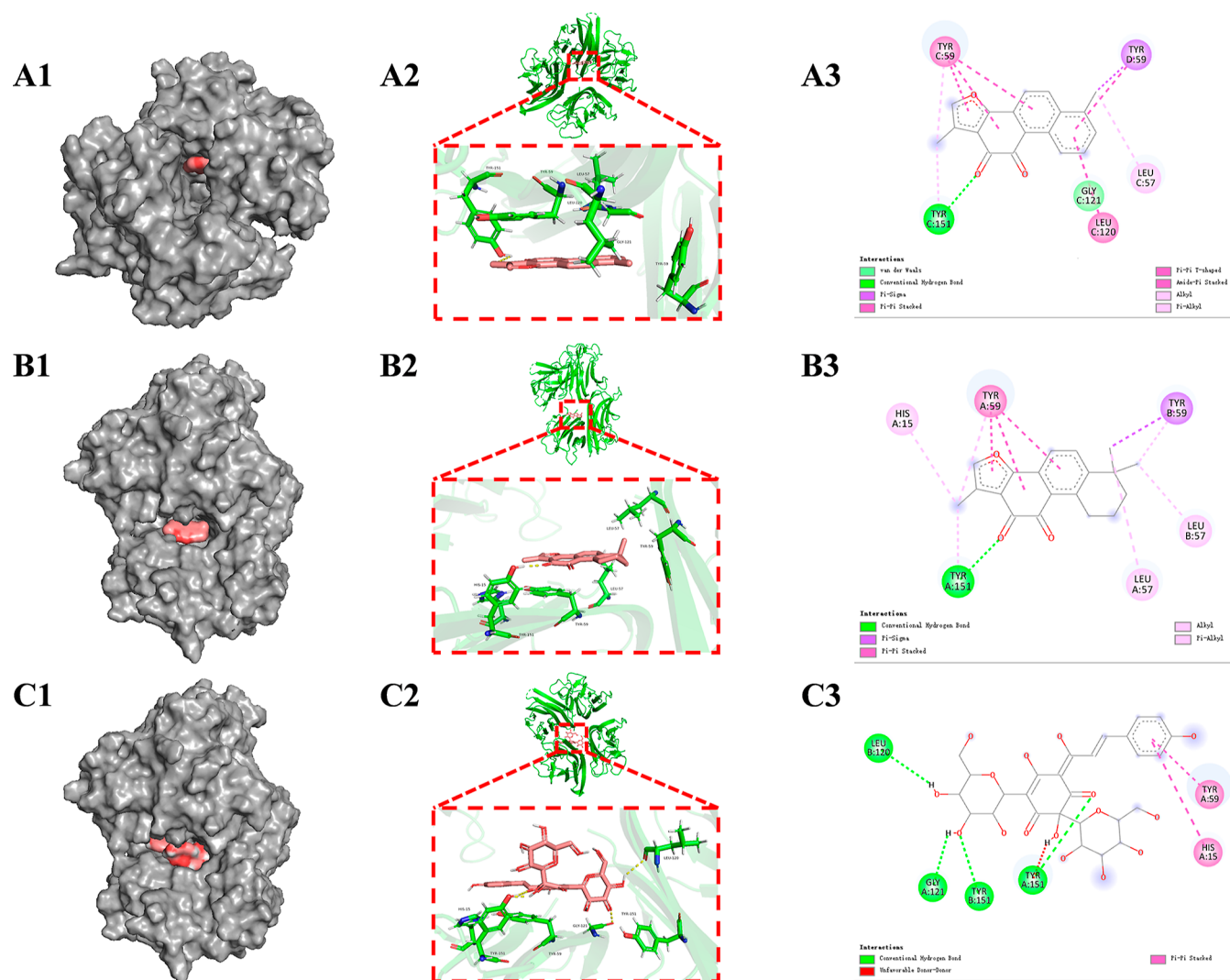


Figure 6. Molecular docking results. (A1) TNF- α -TSl, (A2) TNF- α -TSIIA, and (A3) TNF- α -HSYA: Pocket diagrams. (B1–B3): Three-dimensional patterns of bond, respectively. (C1–C3): Two-dimensional patterns of bond, respectively.

2.12. Statistical Analysis. The data analysis was performed using GraphPad Prism 9.0 software, and the results were presented as the mean \pm standard error of the mean. Statistical significance was determined using a one-way analysis of variance followed by Tukey's multiple comparison test. A significance level of $P < 0.05$ was considered statistically significant.

3. RESULTS

3.1. Identified cDEGs of BD-CI/R. GSE66360 and GSE22255 data sets were finally selected. The GSE66360 data set consists of blood samples from 49 MI patients and 50 healthy volunteers, while the GSE22255 data set includes blood samples from 20 IS patients and 20 healthy volunteers. Both data sets, using microarray technology, obtained gene expression levels of the samples and generated gene expression profiles through Affymetrix Human Genome U133 Plus 2.0 Array. The two data sets were normalized, and then batch effects were removed. The results are listed in Figure 2. In GSE66360, a total of 1144 DEGs were identified, including 635 upregulated and 509 downregulated genes. For GSE22255, 33 DEGs were obtained, with 31 upregulated and 2 downregulated genes. To enhance the clarity of

observing differential gene expression, we generated volcano plots and heat maps for two distinct data sets (Figure 2).

The DEGs were then uploaded to the BioLadder platform separately to generate the Venn diagrams. The Venn diagram showed 26 overlapping upregulated genes and 1 overlapping downregulated gene between the two data sets, resulting in a total of 27 cDEGs of BD-CI/R, as shown in Figure 3 and Table 1.

3.2. Results of GO and KEGG Enrichment Analysis. In the GO analysis, a total of 408 entries were obtained. These entries consisted of 385 BP, 4 Cellular Components (CC), and 19 Molecular Functions (MF). BP was mainly enriched in lipopolysaccharides, cytokine-mediated signaling pathways, inflammatory responses, etc. CC was primarily enriched in transcription factor complexes, transcription regulatory complexes, membrane rafts, etc. MF results indicated that the cDEGs were mainly associated with cytokine activity, chemokine activity, receptor–ligand activity, and binding processes. The KEGG analysis generated 66 signaling pathways, including the IL-17 signaling pathway, TNF signaling pathway, Lipid and atherosclerosis, NF-kappa B signaling pathway, and NOD-like receptor signaling pathway, etc. The top 10 results from GO and KEGG analyses were presented using chord diagrams

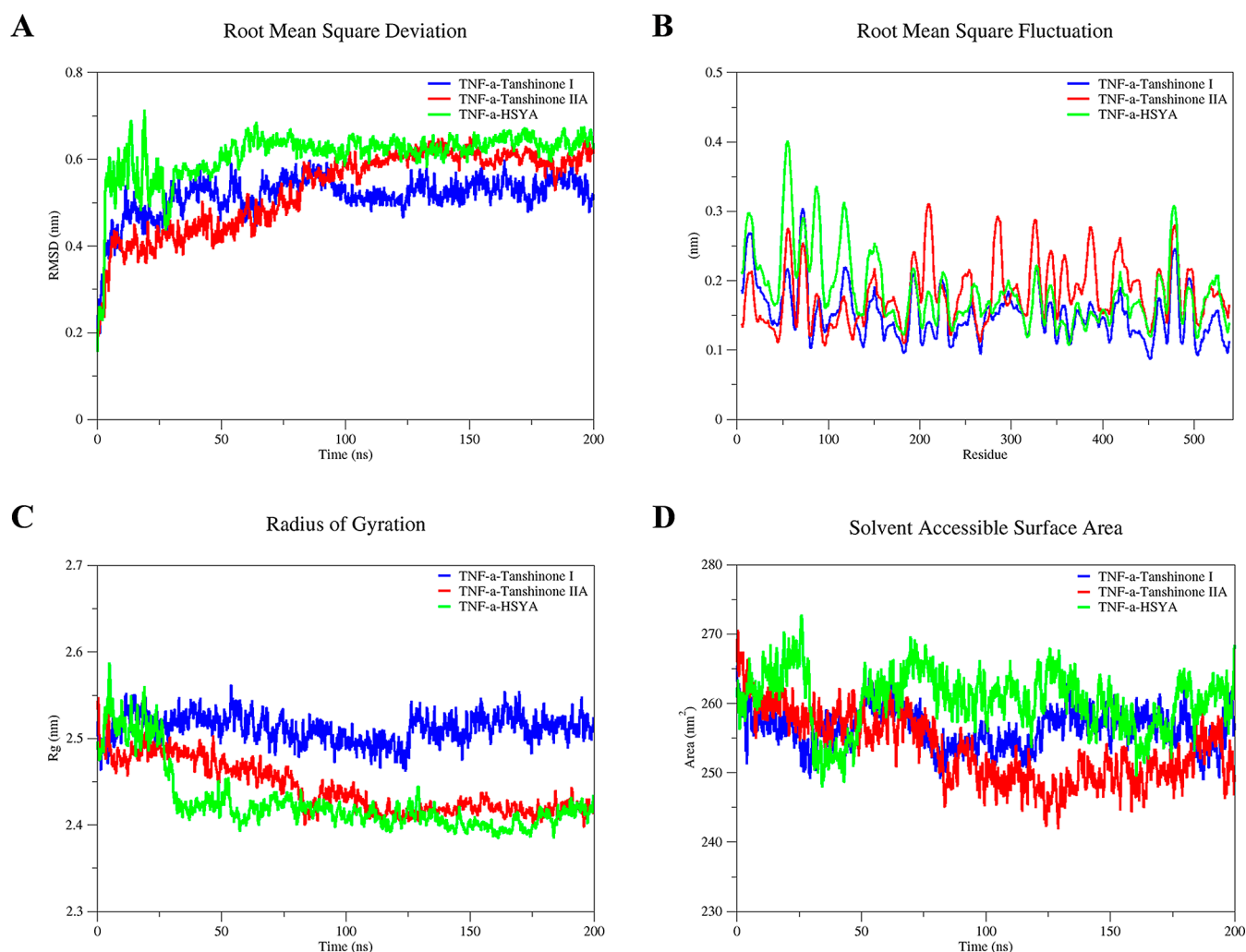


Figure 7. Visualization analysis of molecular dynamics results. (A) RMSD. (B) RMSF. (C) RG. (D) SASA.

(Figure 4A,B). In addition, a KEGG pathway map of the TNF signaling pathway was generated, as shown in Figure 4C.

3.3. Construction of PPI Network. To avoid bias from a single computational method, we employed various Cytoscape plugins, including CytoNCA, MCODE, and cytoHubba, were employed. The PPI networks are shown in Figure 5. By integrating the three computational approaches, TNF was ultimately determined as the key target for BD-CI/R. By querying the UniProt database for the unified names of targets, it is known that the TNF mentioned here corresponds to Tumor Necrosis Factor- α (TNF- α).

3.4. Collection of Active Compounds. Based on the screening criteria, 65 active compounds of DS and 22 active compounds of HH were collected from the TCMSP database. It is worth noting that the OB and DL values are not the only criteria for screening active compounds. By referring to relevant literature,^{44,45} it was discovered that protocatechuic aldehyde, danshensu, salvianolic acid A, and salvianolic acid D, which fall outside the threshold range, possess research value. Therefore, they were added to the sample for further research. Tanshinone I, salvianolic acid B, and Hydroxyl Safflower Yellow A (HSYA) were also supplemented by consulting the Chinese Pharmacopoeia.²⁶ A total of 80 active compounds were obtained after the removal of duplicate and targetless compounds in TCMSP, as shown in Table 2.

3.5. Molecular Docking Results. The 80 collected active compounds were docked respectively to TNF- α (PDB ID: 2AZ5).⁴⁶ Active compounds were screened with a threshold of binding free energy lower than -7 kcal/mol.^{47,48} Table 3 presents the result that 78 active compounds show good binding to TNF- α . Based on the analysis of molecular docking results and the Chinese Pharmacopoeia,²⁶ TSI, TSIIA, and HSYA were ultimately selected for further research. Visualization analysis is shown in Figure 6. TSI was bound to the TYR, LEU, and GLY residues of TNF- α through one hydrogen bond as well as hydrophobic interactions. TSIIA interacted with the HIS, TYR, and LEU residues of TNF- α via one hydrogen bond and hydrophobic interactions. HSYA formed four hydrogen bonds and hydrophobic interactions with the GLY, TYR, LEU, and HIS residues of TNF- α . It is also observed that all three compounds are located in the active site region of TNF- α .

3.6. Validation of the Stability through Molecular Dynamics Simulation. Molecular dynamics simulations were conducted using GROMACS to validate the interactions of TSI, TSIIA, and HSYA with TNF- α . Root mean square deviation (RMSD), Root Mean Square Fluctuation (RMSF), Radius of Gyration (RG), and Solvent Accessible Surface Area (SASA) were separately calculated and visually analyzed. RMSD and RMSF evaluate the binding state and stability of

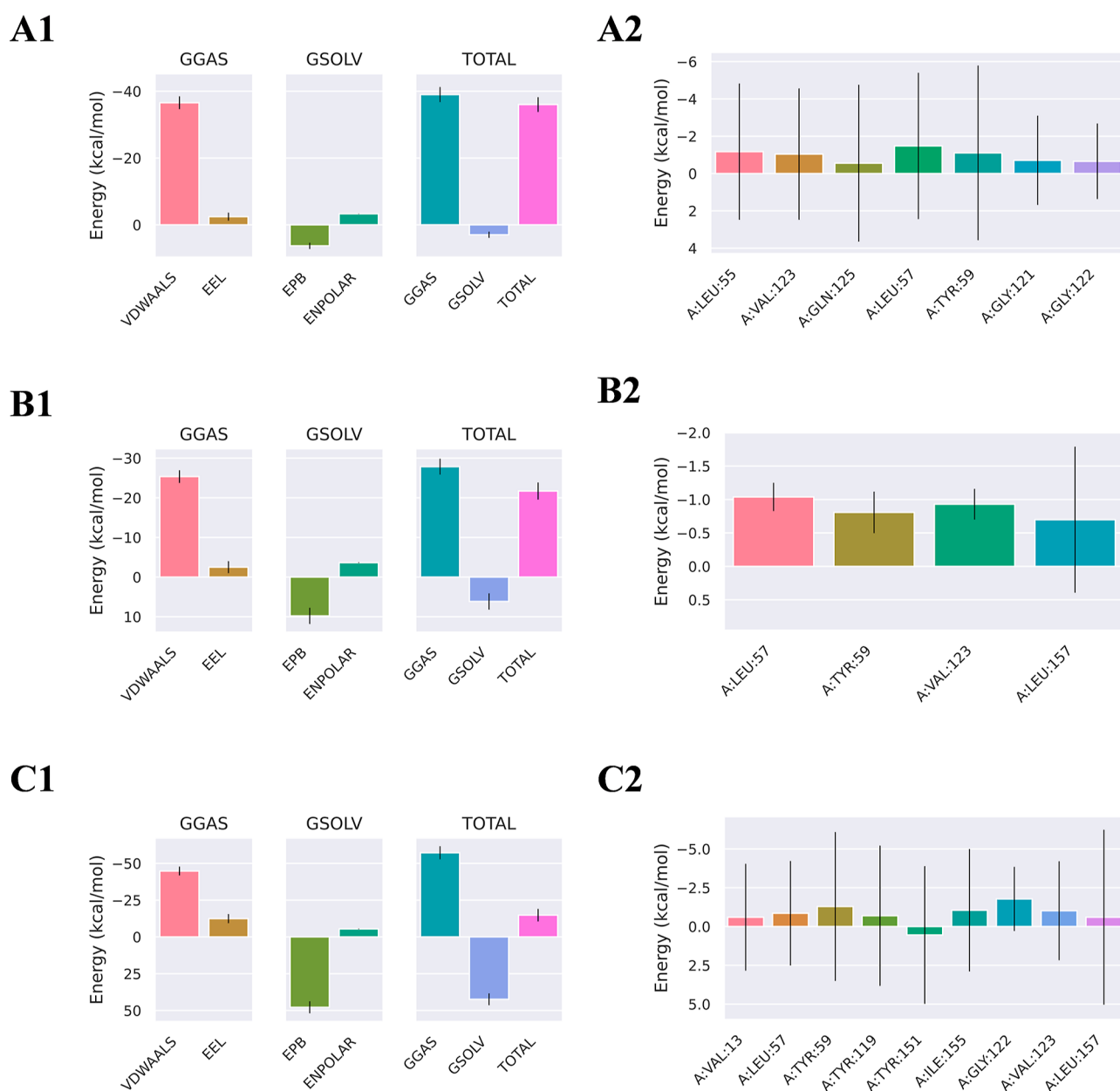


Figure 8. Results of Binding free energies analysis and residue decomposition analysis. (A1) TNF- α -TSI, (A2) TNF- α -TSIIA, and (A3) TNF- α -HSYA: Binding free energies. (B1–B3): Contribution of residue decomposition, respectively.

the protein–ligand complexes, with lower values and lower fluctuations indicating more stable binding.⁴⁹ As shown in Figure 7A, the RMSD of the TNF- α -TSI complex remained relatively stable without large fluctuations. TNF- α -TSIIA complex RMSD became stable after 83 ns, while the TNF- α -HSYA complex RMSD violently fluctuated initially but gradually stabilized after 89 ns. The RMSF values assist in examining the deviation of the ligand from its initial conformation and the motion degree of the protein residues. Greater fluctuations indicate higher instability of the residues, while lesser fluctuations suggest greater stability of the residues.⁵⁰ In Figure 7B, the RMSF values of residues in all three complexes fluctuated within 0.1–0.4 nm, indicating stable overall dynamics. As displayed in Figure 7C, the RG value of the TNF- α -TSI complex fluctuated at 125 ns but became stable afterward. TNF- α -TSIIA and TNF- α -HSYA complexes exhibited similar stable RG values in the midto-end

phase. The SASA value of a protein has long been considered to be one of the key factors affecting protein folding and stability.⁴⁹ In Figure 7D, the SASA value of TNF- α -TSI is relatively stable within 250–265 nm². The SASA value of the TNF- α -TSIIA complex was the lowest, while that of the TNF- α -HSYA complex was the highest. Additionally, greater fluctuations in the SASA value were observed in the TNF- α -HSYA complex. The trends in RG and SASA corroborated the findings from the RMSD analysis.

3.7. Results of MMPBSA Calculations. The binding free energies of TSI, TSIIA, and HSYA with TNF- α were -36.01 , -21.71 , and -14.80 kcal/mol, respectively (Figure 8). TSI interacted with residues LEU55, VAL123, GLN125, LEU57, TYR59, GLY121, and GLY122, among which LEU57 contributed the most. For TSIIA, key residues were LEU57, TYR59, VAL123, and LEU157, with the largest contribution coming from LEU57. Among residues VAL13, LEU57,

Table 4. Results of the ADMET Analysis^a

property	model name	TSI	TSIIA	HSYA	unit
absorption	water solubility	-4.443	-4.494	-2.073	numeric (log mol/L)
	Caco ₂ permeability	1.401	1.419	-0.587	numeric (log P _{app} in 10 ⁻⁶ cm/s)
	intestinal absorption (human)	98.909	96.253	2.705	numeric (% absorbed)
	skin permeability	-2.414	-2.591	-2.735	numeric (log Kp)
	P-glycoprotein substrate	yes	no	yes	categorical (yes/no)
	P-glycoprotein I inhibitor	no	no	yes	categorical (yes/no)
	P-glycoprotein II inhibitor	no	no	no	categorical (yes/no)
distribution	VD _{ss} (human)	0.561	0.325	-0.49	numeric (log L/kg)
	fraction unbound (human)	0.142	0.059	0.414	numeric (Fu)
	BBB permeability	0.447	0.302	-1.391	numeric (log BB)
	CNS permeability	-1.446	-1.494	-5.225	numeric (log PS)
metabolism	CYP2D6 substrate	no	no	no	categorical (yes/no)
	CYP3A4 substrate	yes	yes	no	categorical (yes/no)
	CYP1A2 inhibitor	yes	yes	no	categorical (yes/no)
	CYP2C19 inhibitor	yes	yes	no	categorical (yes/no)
	CYP2C9 inhibitor	no	yes	no	categorical (yes/no)
	CYP2D6 inhibitor	no	no	no	categorical (yes/no)
	CYP3A4 inhibitor	no	no	no	categorical (yes/no)
excretion	total clearance	0.209	0.821	0.865	numeric (log mL/min/kg)
	renal OCT2 substrate	no	no	no	categorical (yes/no)
roxicity	AMES toxicity	yes	no	no	categorical (yes/no)
	max. tolerated dose (human)	-0.116	-0.116	0.011	numeric (log mg/kg/day)
	hERG I inhibitor	no	no	no	categorical (yes/no)
	hERG II inhibitor	no	no	yes	categorical (yes/no)
	oral rat acute toxicity (LD ₅₀)	2.453	2.649	2.671	numeric (mol/kg)
	oral rat chronic toxicity (LOAEL)	2.08	1.885	5.27	numeric (log mg/kg_bw/day)
	hepatotoxicity	no	no	no	categorical (yes/no)
	skin sensitization	no	no	no	categorical (yes/no)
T. pyriformis toxicity	0.645	0.655	0.285	numeric (log ug/L)	
minnow toxicity	-0.148	-0.488	14.756	numeric (log mM)	

^aTSI, tanshinone I; TSIIA, tanshinone IIA; HSYA, Hydroxyl Safflower Yellow A.

Table 5. Drug-Likeness Analysis Results of Tanshinone I, Tanshinone IIA, and HSYA

description	tanshinone I	tanshinone IIA	HSYA
MW	276.08	294.13	612.17
HBD	0	0	12
HBA	3	3	16
logp	2.493	3.247	-2.322
TPSA	43.37	43.37	295.36
Alogp	1.54	0.909	-5.213

TYR59, TYR119, TYR151, ILE155, GLY122, VAL123, LEU157, and GLY122, it is GLY122 that made the greatest contribution to the interaction with HSYA.

3.8. Results of ADMET Analysis. The ADMET analysis was conducted on TSI, TSIIA, and HSYA (Table 4). TSI and TSIIA exhibited higher absorption rates compared to that of HSYA. HSYA was considered to have poor permeability because its intestinal absorption rate is less than 50%.⁵¹ The skin penetration rates of these three compounds are all below -2.5. TSI and HSYA were recognized as substrates for P-glycoprotein, exhibiting increased transport rates and limiting intestinal absorption. VD_{ss} (human), Fraction unbound (human), BBB permeability, and central nervous system (CNS) permeability are commonly used to study drug distribution. HSYA demonstrated a lower VD_{ss} value compared with TSI and TSIIA. Higher VD_{ss} values indicate a wider distribution range and a greater likelihood of

accumulating in target tissues. According to the standards of the pkCSM server,³⁸ compounds have low capability to cross BBB and CNS when logBB is less than -1 and logPS is less than -3. TSI and TSIIA demonstrate good BBB permeability and a good ability to enter the CNS. Regarding metabolism, HSYA was not observed to bind to any cytochrome P450 isoforms, whereas TSI and TSIIA are capable of binding with certain P450 subtypes. Total body clearance of drugs is calculated from hepatic and renal clearances. The analysis revealed clearance rates of 0.209 for TSI, 0.821 for TSIIA, and 0.865 for HSYA. The toxicity analysis indicated that none of the three compounds would cause skin sensitization and hepatic injury. Except for HSYA, TSIA and TSIIA did not exhibit hERG inhibition. Other toxicity-related indicators, AMES toxicity, oral rat acute toxicity (LD₅₀), and oral rat chronic toxicity (LOAEL) were also assessed (Table 4).

3.9. Results of Drug-Likeness Screening. The drug-likeness analysis of TSI, TSIIA, and HSYA was performed based on Lipinski's rule. Table 5 displays the results, indicating that the MW of HSYA is 612.17, which exceeds the threshold of 500, rendering it unable to pass the test. Moreover, HBA and HBD in HSYA significantly surpass the predetermined threshold. This could be attributed to its substantial MW and the existence of multiple torsion angles. TSI and TSIIA all adhere to Lipinski's rule.

3.10. Results of Experimental Verification. Bioinformatics and computer simulation analysis indicate that TNF- α can serve as a key target of BD-CI/R. In the KEGG

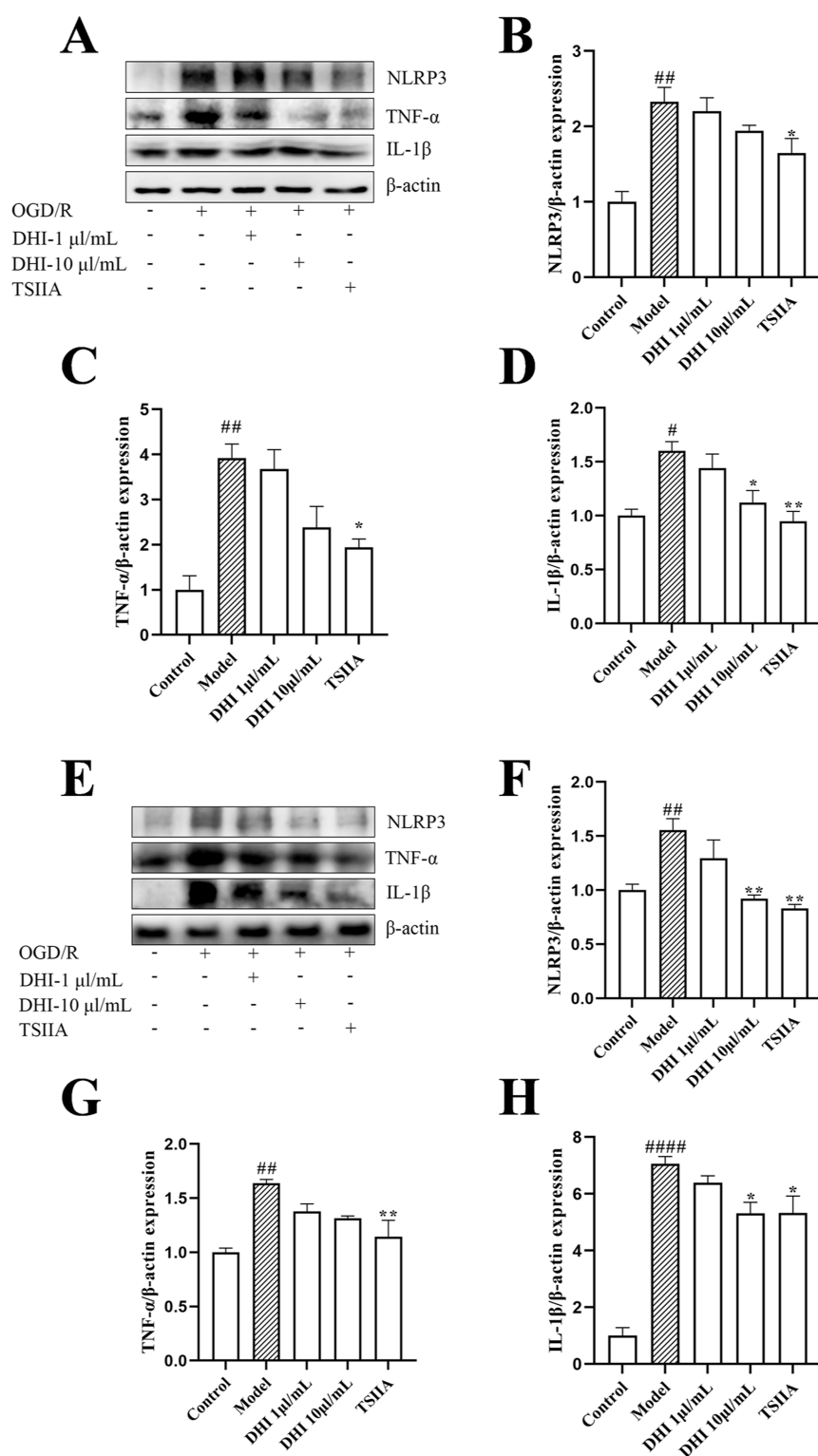


Figure 9. Effect of DHI and TSIIA on the protein levels associated with brain damage caused by cardiac I/R injury. (A) Representative images of TNF- α , NLRP3, and IL-1 β in H9C2 cells. (B–D) The quantitative expression data of TNF- α , NLRP3, and IL-1 β in H9C2 cells. (E) Representative images of TNF- α , NLRP3, and IL-1 β in RBMEC. (F–H) The quantitative expression data of TNF- α , NLRP3, and IL-1 β in RBMEC. [#] $P < 0.05$ vs Control group; ^{*} $P < 0.05$ vs model group.

enrichment analysis, the NOD-like receptor signaling pathway was enriched and ranked highly. TNF- α can activate the NOD-like receptor protein 3 (NLRP3) pathway to release inflammasomes, exacerbating inflammatory damage.⁵² Moreover, relevant studies have shown that NLRP3 is involved in

the occurrence and development of ischemic diseases.^{53,54} Therefore, TNF- α and NLRP3 were selected for further experimental validation. The results are listed in Figure 9. The results showed that the expression levels of TNF- α , NLRP3, and IL-1 β were significantly increased in H9C2 cells after

OGD/R injury. The expression of TNF- α , NLRP3, and IL-1 β was suppressed by treatment with TSIIA. After treatment with DHI (10 μ L/mL), it also exhibited a partial inhibitory effect. Further experimental results showed that the expression levels of TNF- α , NLRP3, and IL-1 β in RBMEC treated with supernatant from OGD/R-H9C2 cells were elevated compared to the control group. It indicated the successful establishment of an in vitro model of BD-CI/R. After treatment with DHI (10 μ L/mL), the expression levels of NLRP3 and IL-1 β were reduced compared to the model group. In the TSIIA group, the expression levels of the three proteins in RBMEC were all decreased.

4. DISCUSSION

Clinically, it has been found that a cardiac I/R injury can cause damage to the brain. Therefore, it is essential to treat the heart and brain together. Our study found that the core target of BD-CI/R was TNF- α . The key active compound of DHI in treating BD-CI/R was TSIIA. DHI and TSIIA can reduce the inflammatory response of BD-CI/R and alleviate damage to the heart and brain.

Bioinformatics methods were used to identify cDEGs of the BD-CI/R. A total of 27 cDEGs were obtained. We discovered a significantly higher number of upregulated genes compared to downregulated ones, consistent with trends observed in previous studies.^{55,56} Enrichment analysis indicated that there is a close association between BD-CI/R and inflammatory response, particularly concerning the IL-17 signaling pathway, TNF signaling pathway, NOD-like receptor signaling pathway, Lipid and atherosclerosis, and others. While an inflammatory response is a short-term protective mechanism, it can lead to adverse effects if it becomes excessive. Therefore regulating the inflammatory response becomes an important approach for treating ischemic diseases.^{57,58} According to the PPI results, the target proteins TNF- α , CXCL8, IL1 β , NFKBIA, and JUN play important roles in the process of BD-CI/R. Among them, TNF- α ranks the highest in overall relevance.

DHI targets antioxidation, anti-inflammatory responses, promotion of angiogenesis, inhibition of platelet aggregation, as well as anticoagulation.^{59,60} Previous studies of DHI have primarily focused on the mechanisms of action in a single disease, with limited research conducted on the mechanisms and core compounds in BD-CI/R. In this study, molecular docking and molecular dynamics simulations were used to screen the active compounds of DHI, and eventually, TSI, TSIIA, and HSYA were selected as the key compounds. The MMPBSA results showed that TSI and TSIIA exhibited the highest binding affinity, whereas HSYA demonstrated the lowest affinity. In addition, we analyzed the contribution of the TNF- α residues during the binding process. Research has revealed that inhibitors bind to residues within the TNF- α dimer, blocking the transition from dimer to trimer to inhibit its activation.⁴⁶ The inhibitors achieve this by binding to residues Leu57, Tyr59, Ser60, Gln61, Tyr119, Leu120, Gly121, Gly122, Tyr151, Leu55, Val123, and Ile155.^{46,61} Our study found that the residues targeted by TSI, TSIIA, and HSYA partially overlap with those targeted by TNF- α inhibitors. This indicates the potential of these three compounds to inhibit the TNF- α activity. ADMET and drug-likeness analysis further verify the pharmacological properties of TSI, TSIIA, and HSYA. TSI and TSIIA outperform HSYA in terms of the MW, TPSA, AlogP, and toxicity. TSI and TSIIA exhibit a lower TPSA value of 43.37, whereas HSYA demonstrates a higher

TPSA value of 295.36. Interestingly, research has unveiled a negative association between TPSA and TNF- α inhibitors.⁶² TSI, TSIIA, and HSYA display AlogP values of 1.54, 0.909, and -5.213, respectively. The greater the AlogP value, the higher the solubility of the compound in organic solvents, indicating a greater lipophilicity.⁶³ In summary, the results of molecular dynamics and binding-free energy are mutually corroborated by pharmacological properties.

In experimental verification, we used the method of transferring the cell supernatant to induce the BD-CI/R model. Transferring cytokines, reactive oxygen species, ions, and other substances released from injured H9C2 cells to RBMEC facilitated construction of a comprehensive injury model.⁴³ Our research indicates that the expressions of TNF- α , NLRP3, and IL-1 β in RBMEC, which have been damaged by OGD/R-H9C2 cells, are significantly increased. Meanwhile, we found that DHI and TSIIA can reduce the inflammatory response of BD-CI/R while alleviating damage to the heart and brain. This suggests that the therapeutic effects of DHI and TSIIA may be mediated through the TNF signaling pathway.

As an important inflammatory cytokine, TNF- α plays a complex role in the occurrence and development of cardiovascular diseases. TNF- α responses involve two receptors: TNFR1 mediates cell apoptosis and inflammation, and TNFR2 mediates tissue repair and regeneration.⁶⁴ Abnormal expression of TNF- α can increase the activity of the NLRP3 inflammasome. Upon activation of the NLRP3 inflammasome, the caspase-1 precursor is triggered, subsequently facilitating the cleavage of pro-IL-1 β by GSDMD.⁶⁵ This process ultimately results in the extracellular release of mature IL-1 β . Moreover, TNF- α can directly activate caspase-1, consequently enhancing the maturation and release of IL-1 β and IL-18.⁶⁶ The inflammasome composed of NLRP3, ASC, and caspase-1 plays a crucial role in the damage and repair of the myocardium and neurons. Studies have found that the activation of the NLRP3 inflammasome accelerates pyroptosis.⁶⁷ In addition, the NLRP3 inflammasome is also involved in ischemic heart disease through inflammation, oxidative stress, myocardial fibrosis, and cardiac remodeling.⁶⁸ NLRP3 is widely present in neurons, microglia, and brain vascular endothelial cells, expanding brain inflammation leading to changes in cell permeability, cell membrane rupture, and cell apoptosis.⁶⁹ Interestingly, the activation of the NLRP3 inflammasome can also increase TNF- α binding to its receptors, exacerbating inflammatory damage.^{70,71} This is a complex and bidirectional reaction process. Hence, it is imperative to investigate the mechanisms of action of TNF- α and NLRP3 in BD-CI/R. Our research demonstrates that BD-CI/R induces pyroptosis in H9C2 cells and RBMEC. DHI and TSIIA decreased the expression of TNF- α , NLRP3, and IL-1 β in BD-CI/R. Computer simulation results and experimental findings confirm that DHI and TSIIA can reduce inflammatory damage and pyroptosis during BD-CI/R through the TNF signaling pathway.

This study relies on bioinformatics and computer simulation techniques to explore the mechanism of DHI treatment for BD-CI/R and verify the results through experiments. However, our study has certain limitations due to time constraints and other factors. Further research on the NLRP3 pathway and nucleotide-binding oligomerization domain like the receptor family is needed in the future.

5. CONCLUSIONS

The results indicate that TNF- α may be the key target that influences BD-CI/R. TSIIA and DHI can reduce the expressions of TNF- α , NLRP3, and IL-1 β in BD-CI/R. The LEU57 residue of TNF- α may have played an important role in the binding process with TSIIA. These findings provide a theoretical basis for future related research.

■ ASSOCIATED CONTENT

SI Supporting Information

The Supporting Information is available free of charge at <https://pubs.acs.org/doi/10.1021/acsomega.4c00200>.

(PDF)

■ AUTHOR INFORMATION

Corresponding Authors

Haitong Wan – School of Basic Medical Sciences, Zhejiang Chinese Medical University, Hangzhou, Zhejiang 310053, China; Key Laboratory of TCM Encephalopathy of Zhejiang Province, Hangzhou, Zhejiang 310053, China; Email: whtong@126.com

Jiehong Yang – School of Basic Medical Sciences, Zhejiang Chinese Medical University, Hangzhou, Zhejiang 310053, China; Key Laboratory of TCM Encephalopathy of Zhejiang Province, Hangzhou, Zhejiang 310053, China; Email: yjhong@zcmu.edu.cn

Authors

Jinfu Wang – School of Basic Medical Sciences, Zhejiang Chinese Medical University, Hangzhou, Zhejiang 310053, China; orcid.org/0009-0006-7553-4025

Yan Guo – Hangzhou TCM Hospital Affiliated to Zhejiang Chinese Medical University, Hangzhou, Zhejiang 310053, China

Huifen Zhou – School of Basic Medical Sciences, Zhejiang Chinese Medical University, Hangzhou, Zhejiang 310053, China; Key Laboratory of TCM Encephalopathy of Zhejiang Province, Hangzhou, Zhejiang 310053, China

Yanjie Hua – College of Life Science, Zhejiang Chinese Medical University, Hangzhou, Zhejiang 310053, China

Complete contact information is available at:

<https://pubs.acs.org/doi/10.1021/acsomega.4c00200>

Author Contributions

[†]J.W. and Y.G. contributed equally to this work.

Notes

The authors declare no competing financial interest.

■ ACKNOWLEDGMENTS

This work was supported by the National Natural Science Foundation of China (no. 82174066, 81973560), the Natural Science Foundation of Zhejiang Province (no. LZ23H270002), and the Key Laboratory of TCM Encephalopathy of Zhejiang Province (no. 2020E10012). Thank you for the support of the above funds and institutions.

■ REFERENCES

(1) Vaduganathan, M.; Mensah, G. A.; Turco, J. V.; Fuster, V.; Roth, G. A. The Global Burden of Cardiovascular Diseases and Risk: A Compass for Future Health. *J. Am. Coll. Cardiol.* **2022**, *80* (25), 2361–2371.

(2) Roth, G. A.; Mensah, G. A.; Johnson, C. O.; Addolorato, G.; Ammirati, E.; Baddour, L. M.; Barengo, N. C.; Beaton, A. Z.; Benjamin, E. J.; Benziger, C. P.; et al. Global Burden of Cardiovascular Diseases and Risk Factors, 1990–2019: Update From the GBD 2019 Study. *J. Am. Coll. Cardiol.* **2020**, *76* (25), 2982–3021.

(3) Yellon, D. M.; Hausenloy, D. J. Myocardial reperfusion injury. *N. Engl. J. Med.* **2007**, *357* (11), 1121–1135.

(4) Bagai, A.; Chen, A. Y.; Udell, J. A.; Dodson, J. A.; McManus, D. D.; Maurer, M. S.; Enriquez, J. R.; Hochman, J.; Goyal, A.; Henry, T. D.; et al. Association of Cognitive Impairment With Treatment and Outcomes in Older Myocardial Infarction Patients: A Report From the NCDR Chest Pain-MI Registry. *J. Am. Heart Assoc.* **2019**, *8* (17), No. e012929.

(5) Apaijai, N.; Moisescu, D. M.; Palee, S.; McSweeney, C. M.; Saiyasit, N.; Maneechote, C.; Boonnag, C.; Chattipakorn, N.; Chattipakorn, S. C. Pretreatment With PCSK9 Inhibitor Protects the Brain Against Cardiac Ischemia/Reperfusion Injury Through a Reduction of Neuronal Inflammation and Amyloid Beta Aggregation. *J. Am. Heart Assoc.* **2019**, *8* (2), No. e010838.

(6) Benjanuwattra, J.; Apaijai, N.; Chunchai, T.; Kerdphoo, S.; Jaiwongkam, T.; Arunsak, B.; Wongsuchai, S.; Chattipakorn, N.; Chattipakorn, S. C. Metformin preferentially provides neuroprotection following cardiac ischemia/reperfusion in non-diabetic rats. *Biochim. Biophys. Acta, Mol. Basis Dis.* **2020**, *1866* (10), 165893.

(7) Yang, Y.; Rosenberg, G. A. Blood-brain barrier breakdown in acute and chronic cerebrovascular disease. *Stroke* **2011**, *42* (11), 3323–3328.

(8) Zhang, T.; Xu, L.; Guo, X.; Tao, H.; Liu, Y.; Liu, X.; Zhang, Y.; Meng, X. The potential of herbal drugs to treat heart failure: The roles of Sirt1/AMPK. *J. Pharm. Anal.* **2024**, *14*, 157–176.

(9) Zhang, H. N.; Zhang, M.; Tian, W.; Quan, W.; Song, F.; Liu, S. Y.; Liu, X. X.; Mo, D.; Sun, Y.; Gao, Y. Y.; et al. Canonical transient receptor potential channel 1 aggravates myocardial ischemia-and-reperfusion injury by upregulating reactive oxygen species. *J. Pharm. Anal.* **2023**, *13* (11), 1309–1325.

(10) Tang, Y. N.; He, X. C.; Ye, M.; Huang, H.; Chen, H. L.; Peng, W. L.; Zhao, Z. Z.; Yi, T.; Chen, H. B. Cardioprotective effect of total saponins from three medicinal species of *Dioscorea* against isoprenaline-induced myocardial ischemia. *J. Ethnopharmacol.* **2015**, *175*, 451–455.

(11) Feng, J. F.; Tang, Y. N.; Ji, H.; Xiao, Z. G.; Zhu, L.; Yi, T. Biotransformation of *Dioscorea nipponica* by Rat Intestinal Microflora and Cardioprotective Effects of Diosgenin. *Oxid. Med. Cell. Longev.* **2017**, *2017*, 4176518.

(12) Zhang, Z.; Dai, Y.; Xiao, Y.; Liu, Q. Protective effects of catalpol on cardio-cerebrovascular diseases: A comprehensive review. *J. Pharm. Anal.* **2023**, *13* (10), 1089–1101.

(13) Fan, H.; Li, M.; Yu, L.; Jin, W.; Yang, J.; Zhang, Y.; Wan, H. Effects of Danhong Injection on platelet aggregation in hyperlipidemia rats. *J. Ethnopharmacol.* **2018**, *212*, 67–73.

(14) Wang, X. P.; Wang, P. F.; Bai, J. Q.; Gao, S.; Wang, Y. H.; Quan, L. N.; Wang, F.; Wang, X. T.; Wang, J.; Xie, Y. D. Investigating the effects and possible mechanisms of danshen- honghua herb pair on acute myocardial ischemia induced by isoproterenol in rats. *Biomed. Pharmacother.* **2019**, *118*, 109268.

(15) He, Q. Y.; Yu, X. Y.; Xiao, Z.; Sun, X.; Zhu, W. F.; Yi, X. Q.; Chen, Q.; Zhang, J. H.; Chen, S. X.; Zhou, X.; et al. Comparison of the Efficacy of Danhong Injections at Different Time-points During the Perioperative Period of Acute Myocardial Infarction: A Systematic Review and Meta-analysis of Randomized Controlled Trials. *Front. Pharmacol.* **2021**, *12*, 643446.

(16) Ma, Y.; Deng, K.; Liu, J.; Ma, B.; Mei, F.; Hui, W.; Luo, X.; Yao, M.; Liu, Y.; Qin, X.; et al. The add-on effects of Danhong injection among patients with ischemic stroke receiving Western medicines: A systematic review and meta-analysis. *Front. Pharmacol.* **2022**, *13*, 937369.

(17) Zhao, J.; Tian, S.; Lu, D.; Yang, J.; Zeng, H.; Zhang, F.; Tu, D.; Ge, G.; Zheng, Y.; Shi, T.; et al. Systems pharmacological study

illustrates the immune regulation, anti-infection, anti-inflammation, and multi-organ protection mechanism of Qing-Fei-Pai-Du decoction in the treatment of COVID-19. *Phytomedicine* **2021**, *85*, 153315.

(18) Valet, G. Cytomics, the human cytome project and systems biology: top-down resolution of the molecular biocomplexity of organisms by single cell analysis. *Cell Prolif.* **2005**, *38* (4), 171–174.

(19) Li, L.; Ma, Q.; Wang, M.; Mou, J.; Han, Y.; Wang, J.; Ye, J.; Sun, G. Single-cell transcriptome sequencing of macrophages in common cardiovascular diseases. *J. Leukoc. Biol.* **2023**, *113* (2), 139–148.

(20) Barrett, T.; Wilhite, S. E.; Ledoux, P.; Evangelista, C.; Kim, I. F.; Tomashevsky, M.; Marshall, K. A.; Phillippy, K. H.; Sherman, P. M.; Holko, M.; et al. NCBI GEO: archive for functional genomics data sets-update. *Nucleic Acids Res.* **2012**, *41* (D1), D991–D995.

(21) Xia, C.; Chen, L.; Sun, W.; Yan, R.; Xia, M.; Wang, Y.; Yang, D. Total saponins from *Paris forrestii* (Takht) H. Li. show the anticancer and RNA expression regulating effects on prostate cancer cells. *Biomed. Pharmacother.* **2020**, *121*, 109674.

(22) Zhou, Y.; Zhou, B.; Pache, L.; Chang, M.; Khodabakhshi, A. H.; Tanaseichuk, O.; Benner, C.; Chanda, S. K. Metascape provides a biologist-oriented resource for the analysis of systems-level datasets. *Nat. Commun.* **2019**, *10* (1), 1523.

(23) Shang, L.; Wang, Y.; Li, J.; Zhou, F.; Xiao, K.; Liu, Y.; Zhang, M.; Wang, S.; Yang, S. Mechanism of Sijunzi Decoction in the treatment of colorectal cancer based on network pharmacology and experimental validation. *J. Ethnopharmacol.* **2023**, *302* (Pt A), 115876.

(24) Szklarczyk, D.; Kirsch, R.; Koutrouli, M.; Nastou, K.; Mehryary, F.; Hachilif, R.; Gable, A. L.; Fang, T.; Doncheva, N. T.; Pyysalo, S.; et al. The STRING database in 2023: protein-protein association networks and functional enrichment analyses for any sequenced genome of interest. *Nucleic Acids Res.* **2023**, *51* (D1), D638–D646.

(25) Ru, J.; Li, P.; Wang, J.; Zhou, W.; Li, B.; Huang, C.; Li, P.; Guo, Z.; Tao, W.; Yang, Y.; et al. TCMSP: a database of systems pharmacology for drug discovery from herbal medicines. *J. Cheminf.* **2014**, *6*, 13.

(26) Chinese Pharmacopoeia Commission. *Chinese Pharmacopoeia of the People's Republic of China*; Vol. 1; The Medicine Science and Technology Press of China: Beijing, China, 2020; pp 77–79.

(27) Chen, G.; Seukep, A. J.; Guo, M. Recent Advances in Molecular Docking for the Research and Discovery of Potential Marine Drugs. *Mar. Drugs* **2020**, *18* (11), 545.

(28) Burley, S. K.; Bhikadiya, C.; Bi, C.; Bittrich, S.; Chao, H.; Chen, L.; Craig, P. A.; Crichlow, G. V.; Dalenberg, K.; Duarte, J. M.; et al. RCSB Protein Data Bank (RCSB.org): delivery of experimentally-determined PDB structures alongside one million computed structure models of proteins from artificial intelligence/machine learning. *Nucleic Acids Res.* **2023**, *51* (D1), D488–D508.

(29) Kim, S.; Chen, J.; Cheng, T.; Gindulyte, A.; He, J.; He, S.; Li, Q.; Shoemaker, B. A.; Thiessen, P. A.; Yu, B.; et al. PubChem 2023 update. *Nucleic Acids Res.* **2023**, *51* (D1), D1373–D1380.

(30) De Vivo, M.; Masetti, M.; Bottegoni, G.; Cavalli, A. Role of Molecular Dynamics and Related Methods in Drug Discovery. *J. Med. Chem.* **2016**, *59* (9), 4035–4061.

(31) Durrant, J. D.; McCammon, J. A. Molecular dynamics simulations and drug discovery. *BMC Biol.* **2011**, *9*, 71.

(32) Berendsen, H. J. C.; van der Spoel, D.; van Drunen, R. GROMACS: A message-passing parallel molecular dynamics implementation. *Comput. Phys. Commun.* **1995**, *91* (1–3), 43–56.

(33) Li, H.; Komori, A.; Li, M.; Chen, X.; Yang, A. W. H.; Sun, X.; Liu, Y.; Hung, A.; Zhao, X.; Zhou, L. Multi-ligand molecular docking, simulation, free energy calculations and wavelet analysis of the synergistic effects between natural compounds baicalein and cubebin for the inhibition of the main protease of SARS-CoV-2. *J. Mol. Liq.* **2023**, *374*, 121253.

(34) Hou, T.; Wang, J.; Li, Y.; Wang, W. Assessing the performance of the MM/PBSA and MM/GBSA methods. 1. The accuracy of binding free energy calculations based on molecular dynamics simulations. *J. Chem. Inf. Model.* **2011**, *51* (1), 69–82.

(35) Lee, S.; Wong, A. R.; Yang, A. W. H.; Hung, A. Interaction of compounds derived from the Chinese medicinal formula Huangqi Guizhi Wuwu Tang with stroke-related numbness and weakness targets: An in-silico docking and molecular dynamics study. *Comput. Biol. Med.* **2022**, *146*, 105568.

(36) Valdes-Tresanco, M. S.; Valdes-Tresanco, M. E.; Valiente, P. A.; Moreno, E. gmx_MMPBSA: A New Tool to Perform End-State Free Energy Calculations with GROMACS. *J. Chem. Theory Comput.* **2021**, *17* (10), 6281–6291.

(37) Ali, S.; Khan, F. I.; Mohammad, T.; Lan, D.; Hassan, M. I.; Wang, Y. Identification and Evaluation of Inhibitors of Lipase from *Malassezia restricta* using Virtual High-Throughput Screening and Molecular Dynamics Studies. *Int. J. Mol. Sci.* **2019**, *20* (4), 884.

(38) Pires, D. E.; Blundell, T. L.; Ascher, D. B. pkCSM: Predicting Small-Molecule Pharmacokinetic and Toxicity Properties Using Graph-Based Signatures. *J. Med. Chem.* **2015**, *58* (9), 4066–4072.

(39) Walters, W. P. Going further than Lipinski's rule in drug design. *Expert Opin. Drug Discovery* **2012**, *7* (2), 99–107.

(40) Lipinski, C. A.; Lombardo, F.; Dominy, B. W.; Feeney, P. J. Experimental and computational approaches to estimate solubility and permeability in drug discovery and development settings IPII of original article: S0169-409X(96)00423-1. The article was originally published in *Advanced Drug Delivery Reviews* 23 (1997) 3–25. 1. *Adv. Drug Deliv. Rev.* **2001**, *46* (1–3), 3–26.

(41) Ertl, P.; Rohde, B.; Selzer, P. Fast calculation of molecular polar surface area as a sum of fragment-based contributions and its application to the prediction of drug transport properties. *J. Med. Chem.* **2000**, *43* (20), 3714–3717.

(42) Leeson, P. D.; Springthorpe, B. The influence of drug-like concepts on decision-making in medicinal chemistry. *Nat. Rev. Drug Discov.* **2007**, *6* (11), 881–890.

(43) Yang, M.; Orgah, J.; Zhu, J.; Fan, G.; Han, J.; Wang, X.; Zhang, B.; Zhu, Y. Danhong injection attenuates cardiac injury induced by ischemic and reperfused neuronal cells through regulating arginine vasopressin expression and secretion. *Brain Res.* **2016**, *1642*, 516–523.

(44) Feng, X.; Li, Y.; Wang, Y.; Li, L.; Little, P. J.; Xu, S. W.; Liu, S. Danhong injection in cardiovascular and cerebrovascular diseases: Pharmacological actions, molecular mechanisms, and therapeutic potential. *Pharmacol. Res.* **2019**, *139*, 62–75.

(45) Qu, C.; Xu, D. Q.; Yue, S. J.; Shen, L. F.; Zhou, G. S.; Chen, Y. Y.; Wang, X. P.; Bai, J. Q.; Liu, F.; Tang, Y. P.; et al. Pharmacodynamics and pharmacokinetics of Danshen in isoproterenol-induced acute myocardial ischemic injury combined with Honghua. *J. Ethnopharmacol.* **2020**, *247*, 112284.

(46) He, M. M.; Smith, A. S.; Oslob, J. D.; Flanagan, W. M.; Braisted, A. C.; Whitty, A.; Cancilla, M. T.; Wang, J.; Lugovskoy, A. A.; Yoburn, J. C.; et al. Small-Molecule Inhibition of TNF- α . *Science* **2005**, *310* (5750), 1022–1025.

(47) Trott, O.; Olson, A. J. AutoDock Vina: improving the speed and accuracy of docking with a new scoring function, efficient optimization, and multithreading. *J. Comput. Chem.* **2010**, *31* (2), 455–461.

(48) Cui, Q.; Zhang, Y. L.; Ma, Y. H.; Yu, H. Y.; Zhao, X. Z.; Zhang, L. H.; Ge, S. Q.; Zhang, G. W.; Qin, X. D. A network pharmacology approach to investigate the mechanism of Shuxuening injection in the treatment of ischemic stroke. *J. Ethnopharmacol.* **2020**, *257*, 112891.

(49) Parihar, A.; Sonia, Z. F.; Akter, F.; Ali, M. A.; Hakim, F. T.; Hossain, M. S. Phytochemicals-based targeting RdRp and main protease of SARS-CoV-2 using docking and steered molecular dynamic simulation: A promising therapeutic approach for Tackling COVID-19. *Comput. Biol. Med.* **2022**, *145*, 105468.

(50) Luo, L.; Zhong, A.; Wang, Q.; Zheng, T. Structure-Based Pharmacophore Modeling, Virtual Screening, Molecular Docking, ADMET, and Molecular Dynamics (MD) Simulation of Potential Inhibitors of PD-L1 from the Library of Marine Natural Products. *Mar. Drugs* **2021**, *20* (1), 29.

(51) Fan, J.; de Lannoy, I. A. Pharmacokinetics. *Biochem. Pharmacol.* **2014**, *87* (1), 93–120.

- (52) Zhao, Y.; Shao, C.; Zhou, H.; Yu, L.; Bao, Y.; Mao, Q.; Yang, J.; Wan, H. Salvianolic acid B inhibits atherosclerosis and TNF- α -induced inflammation by regulating NF- κ B/NLRP3 signaling pathway. *Phytomedicine* **2023**, *119*, 155002.
- (53) Yue, R. C.; Lu, S. Z.; Luo, Y.; Wang, T.; Liang, H.; Zeng, J.; Liu, J.; Hu, H. X. Calpain silencing alleviates myocardial ischemia-reperfusion injury through the NLRP3/ASC/Caspase-1 axis in mice. *Life Sci.* **2019**, *233*, 116631.
- (54) Zhu, H.; Jian, Z.; Zhong, Y.; Ye, Y.; Zhang, Y.; Hu, X.; Pu, B.; Gu, L.; Xiong, X. Janus Kinase Inhibition Ameliorates Ischemic Stroke Injury and Neuroinflammation Through Reducing NLRP3 Inflammasome Activation via JAK2/STAT3 Pathway Inhibition. *Front. Immunol.* **2021**, *12*, 714943.
- (55) Wei, D.; Qi, J.; Wang, Y.; Li, L.; Yang, G.; He, X.; Zhang, Z. NR4A2 may be a potential diagnostic biomarker for myocardial infarction: A comprehensive bioinformatics analysis and experimental validation. *Front. Immunol.* **2022**, *13*, 1061800.
- (56) Zheng, P. F.; Liao, F. J.; Yin, R. X.; Chen, L. Z.; Li, H.; Nie, R. J.; Wang, Y.; Liao, P. J. Genes associated with inflammation may serve as biomarkers for the diagnosis of coronary artery disease and ischaemic stroke. *Lipids Health Dis.* **2020**, *19* (1), 37.
- (57) Gjesdal, O.; Bluemke, D. A.; Lima, J. A. Cardiac remodeling at the population level-risk factors, screening, and outcomes. *Nat. Rev. Cardiol.* **2011**, *8* (12), 673–685.
- (58) Kleinbongard, P.; Heusch, G.; Schulz, R. TNF α in atherosclerosis, myocardial ischemia/reperfusion and heart failure. *Pharmacol. Ther.* **2010**, *127* (3), 295–314.
- (59) Wang, Z.; Wan, H.; Tong, X.; He, Y.; Yang, J.; Zhang, L.; Shao, C.; Ding, Z.; Wan, H.; Li, C. An integrative strategy for discovery of functional compound combination from Traditional Chinese Medicine: Danhong Injection as a model. *Biomed. Pharmacother.* **2021**, *138*, 111451.
- (60) Chen, J.; Cao, W.; Asare, P. F.; Lv, M.; Zhu, Y.; Li, L.; Wei, J.; Gao, H.; Zhang, H.; Mao, H.; et al. Amelioration of cardiac dysfunction and ventricular remodeling after myocardial infarction by danhong injection are critically contributed by anti-TGF- β -mediated fibrosis and angiogenesis mechanisms. *J. Ethnopharmacol.* **2016**, *194*, 559–570.
- (61) Yang, C. Y.; Hung, Y. L.; Tang, K. W.; Wang, S. C.; Tseng, C. H.; Tzeng, C. C.; Liu, P. L.; Li, C. Y.; Chen, Y. L. Discovery of 2-Substituted 3-Arylquinoline Derivatives as Potential Anti-Inflammatory Agents Through Inhibition of LPS-Induced Inflammatory Responses in Macrophages. *Molecules* **2019**, *24* (6), 1162.
- (62) Prasanna, S.; Doerksen, R. J. Topological polar surface area: a useful descriptor in 2D-QSAR. *Curr. Med. Chem.* **2009**, *16* (1), 21–41.
- (63) Roskoski, R. Rule of five violations among the FDA-approved small molecule protein kinase inhibitors. *Pharmacol. Res.* **2023**, *191*, 106774.
- (64) Bouwmeester, T.; Bauch, A.; Ruffner, H.; Angrand, P. O.; Bergamini, G.; Croughton, K.; Cruciat, C.; Eberhard, D.; Gagneur, J.; Ghidelli, S.; et al. A physical and functional map of the human TNF- α /NF- κ B signal transduction pathway. *Nat. Cell Biol.* **2004**, *6* (2), 97–105.
- (65) Zhao, W.; Yang, H.; Lyu, L.; Zhang, J.; Xu, Q.; Jiang, N.; Liu, G.; Wang, L.; Yan, H.; Che, C. GSDMD, an executor of pyroptosis, is involved in IL-1 β secretion in *Aspergillus fumigatus* keratitis. *Exp. Eye Res.* **2021**, *202*, 108375.
- (66) Jain, N.; Sudhakar, C.; Swarup, G. Tumor necrosis factor-alpha-induced caspase-1 gene expression. Role of p73. *FEBS J.* **2007**, *274* (17), 4396–4407.
- (67) Huang, Y.; Xu, W.; Zhou, R. NLRP3 inflammasome activation and cell death. *Cell. Mol. Immunol.* **2021**, *18* (9), 2114–2127.
- (68) Zhaolin, Z.; Guohua, L.; Shiyuan, W.; Zuo, W. Role of pyroptosis in cardiovascular disease. *Cell Prolif.* **2019**, *52* (2), No. e12563.
- (69) Long, J. X.; Tian, M. Z.; Chen, X. Y.; Yu, H. H.; Ding, H.; Liu, F.; Du, K. The role of NLRP3 inflammasome-mediated pyroptosis in ischemic stroke and the intervention of traditional Chinese medicine. *Front. Pharmacol.* **2023**, *14*, 1151196.
- (70) Peng, L.; Lei, Z.; Rao, Z.; Yang, R.; Zheng, L.; Fan, Y.; Luan, F.; Zeng, N. Cardioprotective activity of ethyl acetate extract of *Cinnamomi Ramulus* against myocardial ischemia/reperfusion injury in rats via inhibiting NLRP3 inflammasome activation and pyroptosis. *Phytomedicine* **2021**, *93*, 153798.
- (71) Huang, Z.; Zhou, X.; Zhang, X.; Huang, L.; Sun, Y.; Cheng, Z.; Xu, W.; Li, C. G.; Zheng, Y.; Huang, M. Pien-Tze-Huang, a Chinese patent formula, attenuates NLRP3 inflammasome-related neuroinflammation by enhancing autophagy via the AMPK/mTOR/ULK1 signaling pathway. *Biomed. Pharmacother.* **2021**, *141*, 111814.